AD-A250 556

MENTATION PAGE

1. AGENCY USE ONLY (Leave blank)	2. REPORT DATE 1991	3. REPORT TYPE AND DATES COVERED THESIS/DISSERTATION

4. TITLE AND SUBTITLE	5. FUNDING NUMBERS
Microwave Derived Rainrates in Typhoons and Their Use in the Diagnosis and Prediction of Typhoon Intensity	

6. AUTHOR(S)

Paul D. MacArthur, Capt

7. PERFORMING ORGANIZATION NAME(S) AND ADDRESS(ES)	8. PERFORMING ORGANIZATION REPORT NUMBER
AFIT Student Attending: St. Louis University	AFIT/CI/CIA-91-118

9. SPONSORING/MONITORING AGENCY NAME(S) AND ADDRESS(ES)	10. SPONSORING/MONITORING AGENCY REPORT NUMBER
AFIT/CI Wright-Patterson AFB OH 45433-6583	

11. SUPPLEMENTARY NOTES

12a. DISTRIBUTION/AVAILABILITY STATEMENT	12b. DISTRIBUTION CODE
Approved for Public Release IAW 190-1 Distributed Unlimited ERNEST A. HAYGOOD, Captain, USAF Executive Officer	

13. ABSTRACT (Maximum 200 words)

DISTRIBUTION STATEMENT A
Approved for public release!
Distribution Unlimited

DTIC
ELECTE
MAY 11 1992
S B D

14. SUBJECT TERMS			15. NUMBER OF PAGES
			81
			16. PRICE CODE

17. SECURITY CLASSIFICATION OF REPORT	18. SECURITY CLASSIFICATION OF THIS PAGE	19. SECURITY CLASSIFICATION OF ABSTRACT	20. LIMITATION OF ABSTRACT

NSN 7540-01-280-5500

Standard Form 298 (Rev. 2-89)

ABSTRACT

An algorithm to convert satellite measured microwave radiances to rainfall rates was used to analyze the rainfall patterns of western North Pacific Ocean typhoons. These rainfall rates and patterns were correlated to the typhoon's Dvorak intensities (both present and future) in search of diagnostic insights and prognostic aids.

The number of local maxima of mean annular rainrates correlated strongly with the filling or deepening of a typhoon. Storms with multiple peaks filled, indicating the existence of the barrier effect. An *effective radius* which demarks two regions where latent heat release either raises or depresses the central pressure was postulated.

Cross-sections of convective and stratiform rainfall indicated both the importance of stratiform rain and the need for an active convective core in growing typhoons. The ratio of convective to total precipitation also showed the importance of stratiform rain to storm intensification and illustrated the *barrier effect.*

Finally, northwesterly moving typhoons were examined in detail. Stable regression estimates of storm intensification were found.

MICROWAVE DERIVED RAINRATES

IN TYPHOONS AND THEIR USE IN THE

DIAGNOSIS AND PREDICTION OF TYPHOON INTENSITY.

Paul Douglas MacArthur, B.S., Captain, USAF

1991

81 pages

Master of Science (Research)
St. Louis University

92-11943

02 5 01 027

MICROWAVE DERIVED RAINRATES

IN TYPHOONS AND THEIR USE IN THE

DIAGNOSIS AND PREDICTION OF TYPHOON INTENSITY.

Paul Douglas MacArthur, B.S., Captain, USAF

1991

81 pages

Master of Science (Research)
St. Louis University

REFERENCES

Adler, R.F., R.A. Mack, N. Prasad, H.-Y.M. Yeh, and
I.M. Hakkarinen, 1990: Aircraft microwave
observations and simulations of deep convection
from 18 to 183 GHz. Part I: Observations.
Journal of Atmospheric and Oceanic Technology, 7,
377-391.

Burpee, R.W., and M.L. Black, 1989: Temporal and
spatial variations of rainfall near the centers of
two tropical cyclones. *Mon. Wea. Rev.*, 117, 2204-
2218.

Carr, L.E. III, and R.L. Elsberry, 1990: Observational
evidence for predictions of tropical cyclone
propagation relative to environmental steering.
J. Atmos. Sci., 47, 542-546.

Dvorak, V.F., 1984: Tropical cyclone intensity
analysis using satellite data. NOAA technical
report NESDIS 11. US Department of Commerce,
Washington D.C., 47pp.

Fiorino, M., and R.L. Elsberry, 1989a: Contributions
to tropical cyclone motion by small, medium and
large scales in the initial vortex. *Mon. Wea.
Rev.*, 117, 721-727.

_____, and _____, 1989b: Some aspects of
vortex structure related to tropical cyclone
motion. *J. Atmos. Sci.*, 46, 975-990.

Glass, M., and G.W. Felde, 1989: Structure of tropical
cyclones and surrounding regions as determined
from OLS and SSM/I imagery analysis. *Preprints.
Fourth Conference on Satellite Meteorology and
Oceanography*, San Diego, California, American
Meteorology Society, Boston, Ma., 35-38.

Hoffman, C.W., V.G. Patterson, and D.J. McMorrow, 1988:
1987 annual tropical cyclone report. Joint
Typhoon Warning Center, Guam, Mariana Islands,
213pp.

Holland, G.J., 1983: Tropical cyclone motion:
Environmental interaction plus betta effect. *J.
Atmos. Sci.*, 40, 328-342.

Hollinger, J.T., K. Lo, G. Poe, R. Savage, and J.
Peirce, 1987: Special sensor microwave/imager
user's guide. Dept of the Navy, Naval Research
Lab., Washington, D.C., 120 pp.

Jorgensen, D.P., 1984: Mesoscale and convective scale characteristics of mature hurricanes. Part I: General observations by research aircraft. *J. Atmos. Sci.*, **41**, 1268-1285.

Merril, R.T., 1988: Environmental influences on hurricane intensification. *J. Atmos. Sci.*, **45**, 1678-1687.

Olson, W.S., F.J. Fontaine, W.L. Smith, and T.H. Achtor, 1990: Recommended algorithms for the retrieval of rainfall rates in the tropics using SSM/I (DMSP-8). Manuscript, Univ. of Wisconsin, Madison. 10pp.

Plante, R.J. and D.J. McMorrow, 1989: 1988 annual tropical cyclone report. Joint Typhoon Warning Center, Guam, Mariana Islands, 216pp.

Powell, M.D., 1990: Boundary layer structure and dynamics in outer hurricane rainbands part I: Mesoscale rainfall and kinematic structure. *Mon. Wea. Rev.*, **118**, 891-917.

_____, and P.G. Black, 1984: Airborne Doppler radar observations of the boundary layer of Hurricane Debby (1982). *Preprints, 22nd Conf. on Radar Meteorology*. Zurich, Switzerland, Amer. Meteor. Soc., Boston, 584 - 588.

Rao, A.V.R.K., R.R. Kelkar, and P.A. Arkin, 1989: Estimation of precipitation and outgoing longwave radiation from INSAT-IB radiance data. *Mausam*, **40**, 123-130.

Rao, G.V., 1970: An analytical study of the differential frictional effect on vortex movement. *Mon. Wea. Rev.*, **98**, 1332-135.

_____, E.J. Ciardi and D.K. Rhudy, 1989: Comparison of SSM/I rainrates and surface winds with the corresponding conventional data in the north west pacific typhoons. *Preprints. Fourth Conference on Satellite Meteorology and Oceanography*, San Diego, California, American Meteorology Society, Boston, Ma., 104-107.

Rhudy, D.K., 1989: Applications of microwave radiometric measurements to infer tropical cyclone intensity and strength. M.S. Thesis, St. Louis University, St. Louis, Mo., 95 pp. Available from University Microfilms, Ann Arbor, Mi.

Spencer, R.W., H.M. Goodman, and R.E. Hood, 1989:
    Precipitation retreval over land and ocean with
    SSM/I: Identification and characteristices of the
    scattering signal. *Journal of Atmospheric and
    Oceanic Technology*, 6, 254-273.

Staff, 1988: Tropical cyclones in 1987. Royal
    Observatory, Hong Kong, 73pp.

Steranka, J., E.B. Rodgers, and R.C. Gentry, 1986: The
    relationship between Satellite measured convective
    bursts and tropical cyclone intensification. *Mon.
    Wea. Rev.*, 114, 1539-1546.

Willoughby, H.E., 1988: Dynamics of the tropical
    cyclone core. *Aust. Met. Mag.*, 36, 183-191.

MICROWAVE DERIVED RAINRATES

IN TYPHOONS AND THEIR USE IN THE

DIAGNOSIS AND PREDICTION OF TYPHOON INTENSITY.

Paul Douglas MacArthur, B.S.

A Digest Presented to the Faculty of the Graduate
School of Saint Louis University in Partial
Fulfillment of the Requirements for the
Degree of Master of Science (Research)

1991

DIGEST

An algorithm to convert satellite measured microwave radiances to rainfall rates was used to analyze the rainfall patterns of western North Pacific Ocean typhoons. These rainfall rates and patterns were correlated to the typhoon's Dvorak intensities (both present and future) in search of diagnostic insights and prognostic aids.

SSM/I data proved useful in predicting the intensification and future central pressure of typhoons. The number of peaks in the mean annular rainfall rates correlated strongly with the filling or deepening of a typhoon. Storms with multiple peaks filled, indicating the existence of the barrier effect. Case studies of Lynn and Dinah (1987) showed a strong correlation between rainfall and 24-h central pressure. It is hypothesized that the radius of maximum correlation indicates the location of the "effective radius."

Cross-sections of convective and stratiform rainfall statistics were stratified into four classes of intensification. The patterns depicted in the cross-section class composites indicated the importance of stratiform rain and the need for an active convective core in a growing typhoon. The PIP, defined as the ratio between convective and total precipitation

also showed the importance of stratiform rain to storm intensification and illustrated the "barrier effect." Storms with convectively active outer regions weakened since moisture rich air was blocked from reaching the core by the convection.

Finally, the typhoons were stratified by direction of movement, and the northwesterly movers were examined in detail. Stable regression estimates of storm intensification in terms of mean rainfall rates and PIP were found.

MICROWAVE DERIVED RAINRATES

IN TYPHOONS AND THEIR USE IN THE

DIAGNOSIS AND PREDICTION OF TYPHOON INTENSITY.

Paul Douglas MacArthur, B.S.

A Thesis Presented to the Faculty of the Graduate
School of Saint Louis University in Partial
Fulfillment of the Requirements for the
Degree of Master of Science (Research)

1991

COMMITTEE IN CHARGE OF CANDIDACY:

Professor Gandikota V. Rao,
        Chairperson and Advisor

Assistant Professor Lawrence Coy

Associate Professor James T. Moore

ACKNOWLEDGEMENTS

TABLE OF CONTENTS

LIST OF TABLES

LIST OF ILLUSTRATIONS

1. INTRODUCTION

Typhoons, hurricanes, and tropical storms are in every sense important meteorological phenomena. They play a significant role in the global energy budget, carrying great quantities of energy rich air poleward. Unfortunately, in their tracks toward the subtropics, they adversely impact human life and livelihood. In 1987 the western North Pacific had six super typhoons (maximum sustained surface winds of at least 130 kts), 12 typhoons, and six tropical storms. Their effect on human life is summarized in Table 1.1. Climatologically 1987 was a light year with only 24 tropical storms verses a mean of 30.7 per year. The importance of understanding and possibly predicting these storms, therefore, is clear.

On 1 October 1987 the United States Air Force ceased areal reconnaissance of tropical cyclones in the western Pacific ocean. This vacuum was filled by satellite observations. Satellites remain the prime source of tropical storm observations today. Several spectra are sensed by these satellites' sensors. The most common are the visual and infrared regions, however, the constellation is rapidly gaining radiometers with microwave sensing capability.

This paper will examine the process of converting microwave radiances over ocean to rainrates. It will

1

Table 1.1. List of 1987 typhoons which had significant human costs. Numbers do not include lost time or travel and shipping delays. Figures are from JTWC annual tropical cyclone report.

Storm	Location	Human loss	Material loss
Thelma	Korea	Many dead	Extensive
Wynne	Marianas		Extensive
Alex	Korea	Many dead	Major floods
Betty	Philippines	20–27 dead 60,000 homeless	$millions
Dinah	Japan		$millions
Gerald	Taiwan China	5 dead 122 dead	$millions $millions
Lynn	Taiwan	42 dead 18 missing	$millions
Nina	Truk Atoll Philippines	5 dead 40,000 homeless 687 dead 500,000 homeless	$30–40 \times 10^6
Phyllis	Philippines	10–23 dead	

seek respective correlations between convective and non-convective rainfall rates and storm characteristics. Similarly, typhoon development trends also will be examined and correlations determined. Additionally, it will investigate the relation of the location of convective bands, and the relative distribution of convective vs. stratiform rain to typhoon characteristics and intensity trends. Specifically the experiments contained in this paper are:

1) The deepening of typhoons as revealed by mean annular rainfall rates. Mean annular rainfall rates indicate rainband formation. When multiple layers of rainbands form it is likely that the storm is weakening.

2) The life cycles of Typhoons Lynn and Dinah (both 1987). Rainfall rates seem to have a strong inverse relationship to the future central pressure of typhoons. Connections to the concept of effective radius are explored too.

3) Statistical cross-sections of convective and stratiform rainfall within typhoons. Typhoons are divided into four stages of deepening (or filling) and rainfall patterns are exposed which are associated with each stage.

4) The relative distribution of convective vs. stratiform rain in connection to typhoon deepening and

future central pressure. Strong convective activity relative to stratiform rainfall is tied both to the strengthening and destruction of typhoons, depending on where the activity is located.

5) The examination of typhoons which move to the northwest. Mean and total rainfall rates of convective, stratiform, and combined rain are compared against deepening and future pressure.

Other experiments are mentioned which failed to yield strong correlations. It is hoped that future work will help explain these failures, as well as to expand on the five successes.

2. REVIEW OF RELATED MATERIAL

Many articles have been written about the nature of typhoons and/or hurricanes. These papers provide valuable background knowledge to those wishing to understand tropical storms. Jorgensen (1984) examined precipitation features in the eye wall, the stratiform region adjacent and outside of the eye wall, and the rainbands (convective and stratiform), noting that precipitation outside the eye wall was predominately stratiform. Burpee and Black (1989) found, in radar studies of two hurricane eye regions, that the rainrate was highly variable due to growth and motion of convective cells. Steranka et al. (1986) found that cloud top temperatures and future maximum winds of Atlantic hurricanes could be correlated. They also noted that convective surges developed around the eye (within 222 km) preceding the increase of maximum winds (as determined by Best Track data). Powell and Black (1984) indicated that the effects of a principle rainband may act as a barrier to high theta-e air. As a result of hurricane planetary boundary experiments, Powell (1990) found that Powell and Black's (1984) barrier effect may be important in controlling the inflow of unstable air into the eye wall. The rainband updraft influenced the hurricane's planetary boundary layer and the surrounding vergence and subsidence.

Merril (1988) showed that the hurricane vortex is influenced by external factors. He noted three parameters which would influence the growth of hurricanes. These parameters are sea surface temperature, the influx of absolute angular momentum, and upper level outflow patterns.

Several authors have examined tropical cyclone motion. Rao (1970), Carr and Elsberry (1990), and Fiorino and Elsberry (1989a, 1989b) modeled vortex motion in a tropical context. Most important to this study, Holland (1983) modeled tropical cyclone motion in an effort to explain the discrepancy between Rossby theory and observations. In his study he introduced the "effective radius" which is given to be between 200 and 400 km. Within this radius the storm is shielded from the effects of the environment.

Attempts have been made to use meteorological satellite data in tropical storm research. Rao, Kelkar, and Arkin (1989) described methodologies of computing quantitative precipitation estimates from outgoing longwave radiation (OLR), and showed its validity for tropical oceanic storms.

Application of microwave data followed the addition of microwave radiometers to meteorological satellite sensors. Previously, microwave data had been gathered primarily from airborne platforms. Adler et al. (1990) used aircraft mounted radiometers to

measure the 18 to 183 GHz spectra. They were able to detect extreme updrafts and convective cores through Brightness Temperatures (TBs).

Dvorak (1984) suggested a method of gauging tropical storm intensity through satellite analysis. This method is used by the Joint Typhoon Warning Center (JTWC) which provides Best Track and Fix data for use (among other things) in typhoon studies. The Best Track data (Holland et al. 1988 and Plante et al. 1989) provided the "truth" in our research. Data of Defense Meteorological Satellite Program (DMSP) satellite borne Special Sensor Microwave/ Imager (SSM/I) was compared to visible (Vis) and infrared (IR) data by Glass and Felde (1989). They showed the superiority of SSM/I data over infrared in depicting convective cells embedded within an oceanic hurricane. They found 85 GHz data revealed well defined rainbands where Vis and IR only showed a loosely organized system of cells. The microwave sensors were also shown to be consistent with model output.

Rhudy (1989) applied SSM/I data to determine typhoon strength and intensity. He found there was a correlation between intensity and latent heat release as implied by the rainfall records in the Environmental Data Records (EDR). The EDR rainfall rates are determined by a linear algorithm developed by Hughes Aircraft Company. He also examined the precipitation

intensity parameter (PIP) for use as an intensity indicator. The PIP is a parameter that measures the fractional contribution of convective rain to the storms total. Rhudy used a 5 mm/hr definition of convective intensity where Willoughby (1988) defined convective rainfall as rain rates from 3 to 30 rm/hr. Since the concept of Rhudy's PIP was well founded in theory, we will reexamine PIP and similar concepts with Willoughby's definition of convective rainfall.

Rao, Ciardi, and Rhudy (1989) calculated the latent heat release in typhoon Lynn (1987), using SSM/I derived rainrates. They compared radar and SSM/I rainfall rates for typhoon Lynn and noted a moderate correlation (r=.49, N=125).

Olson et al. (1990) improved the SSM/I rainrate algorithm by replacing it with a non-linear combination of five microwave frequencies. They tested the new algorithm by comparing its rainfall rates against a "truth" of rainfall rates from airborne radar. Their results were markedly better (r = .772 N = 1365) than Rao, Ciardi, and Rhudy (1989). Armed with this new algorithm, we will continue to explore the applicability of the satellite gathered microwave data to forecasting the characteristics and behavior of tropical storms.

3. THE SPECIAL SENSOR MICROWAVE/ IMAGER AND DATA

In 1987 the United States Department of Defense launched the DMSP satellite F8. F8 has a polar orbit with an orbital inclination of 98.8 degrees and period of 102 minutes. It makes 14.1 sun-synchronous orbits per day, advancing westward about 25.5 degrees longitude on the equator on each ascent.

DMSP satellite F8 carries the Special Sensor Microwave/ Imager (SSM/I). This sensor measures upwelling linearly polarized microwave radiance in seven channels. They are: 19 GHz vertically (V) and horizontally (H) polarized, 22V, 37 V and H, and 85 V and H. Radiances are measured and converted to Brightness Temperatures.

Microwave radiances come from three sources: atmospheric and surface emissions, and atmospheric emissions reflected by the surface. These emissions are attenuated as they pass through the atmosphere. Thus, unlike infrared and visual data, microwave data generally represent an atmospheric layer of considerable depth. Water clouds and rainfall increase emissions, thus improving data quality, instead of acting as a mask. Cirrus is transparent, enabling observation of the often covered eye.

Brightness Temperature is an approximation of the Black Body Temperature in the the microwave frequency

domain. In this domain, hv/KT << 1 so the Plank formula:

$$B_v(T) = 2hv^3 / [c^2 (e^{hv/kT} - 1)] \qquad (1)$$

is approximated as:

$$B_v(T) = (2kv^2 / c^2) T \qquad (2)$$

Where: $B_v(T)$ is the Plank function in the frequency domain,

     h is Plank's constant (6.626×10^{-27} erg sec),

     v is frequency (Hz),

     c is the speed of light (2.998×10^{10} cm sec^{-1}),

     k is Boltzmann's constant (1.381×10^{-16} erg deg^{-1}), and

     T is the Black Body temperature (K).

This linear approximation can be expressed in terms of radiance (I_v, which SSM/I measures) and Brightness Temperature (TB or T_B), such that:

$$I_v = (2kv^2/c^2) T_B(v). \qquad (3)$$

or

$$T_B(v) = I_v (c^2/2kv^2) \qquad (4)$$

Figure 3.1 illustrates the scan geometry of SSM/I. The SSM/I scans along a plane which is sloped 45° to the aft of F8, scanning 51.2° on either side of the sub-satellite track. This produces a scanned swath 1400 km long and 12.5 km wide. Only the 85 GHz frequency is sensed every scan. The other frequencies are sensed on alternating scans. In addition, only the 85 GHZ channels divide the scan into 128 discrete measurements, the others divide the scan into 64 points. Table 3.1 lists the effective fields of view (EFOV) of each channel's scan points. The difference in the EFOV between frequencies is due partly to the measurement period, but largely to the precision of the radiometers comprising SSM/I. The least precise channels have a greater data overlap than the more precise channels: Fig. 3.2 demonstrates the differences in data overlap. Clearly, 85 GHz is the most precise and 19 GHZ is the least precise scanning frequency.

Brightness Temperatures from each channel and scan rotation are simultaneously transmitted to ground stations and stored in memory. These data (Sensor Data Records, or SDRs) are routinely transmitted to special ground stations for placement in archives. SDRs are labeled by the orbit number of transmission time when placed in the archives.
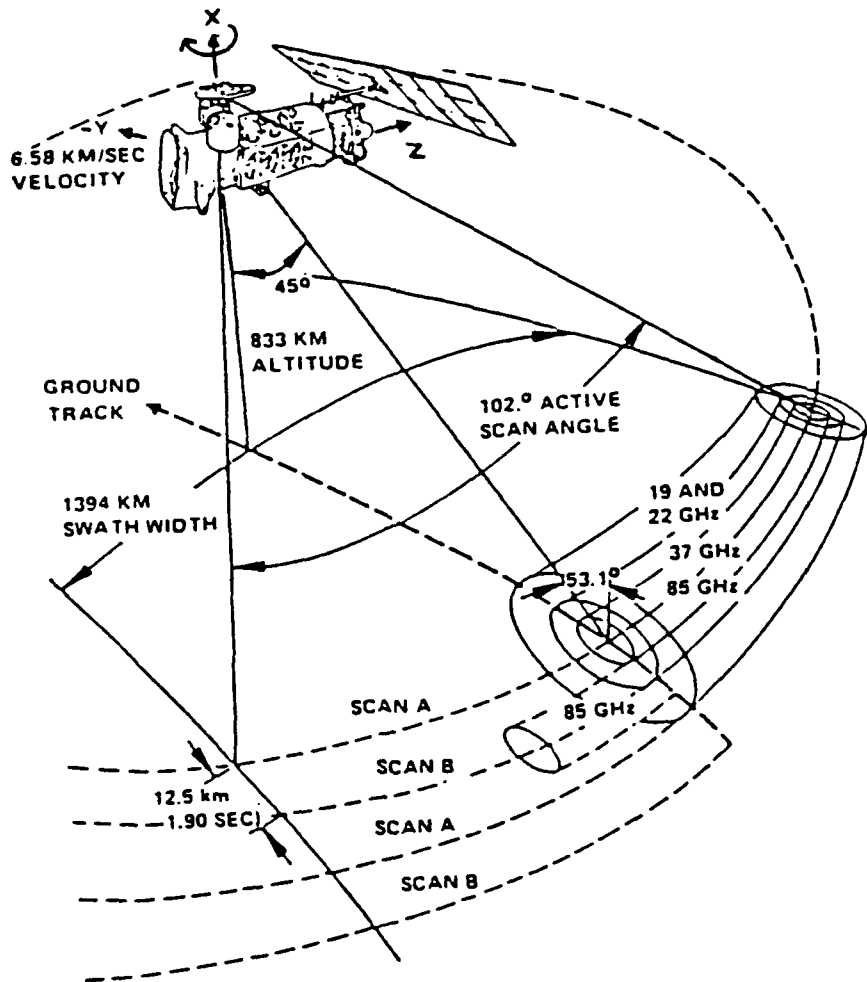
Figure 3.1. Scan geometry of SSM/I radiometers. Note that only the 85GHz channels are processed for both scans A and B, all other channels are only scanned during A scans. From Hollinger et al. (1987).

Table 3.1. List of SSM/I channel characteristics, including frequency, polarization, and Effective Fields of View (EFOV). Surface EFOVs are shown in more detail in figures A and A.1. After Hollinger et al. (1987).

Frequency (GHz)	Pol	Beamwidth EFOV (degree)	Surface EFOV	
			Along track (km)	Cross track (km)
19.35	V	1.93	69	43
19.35	H	1.93	69	43
22.235	V	1.83	50	40
37.0	V	1.27	37	28
37.0	H	1.31	37	29
85.5	V	0.60	15	13
85.5	H	0.60	15	13
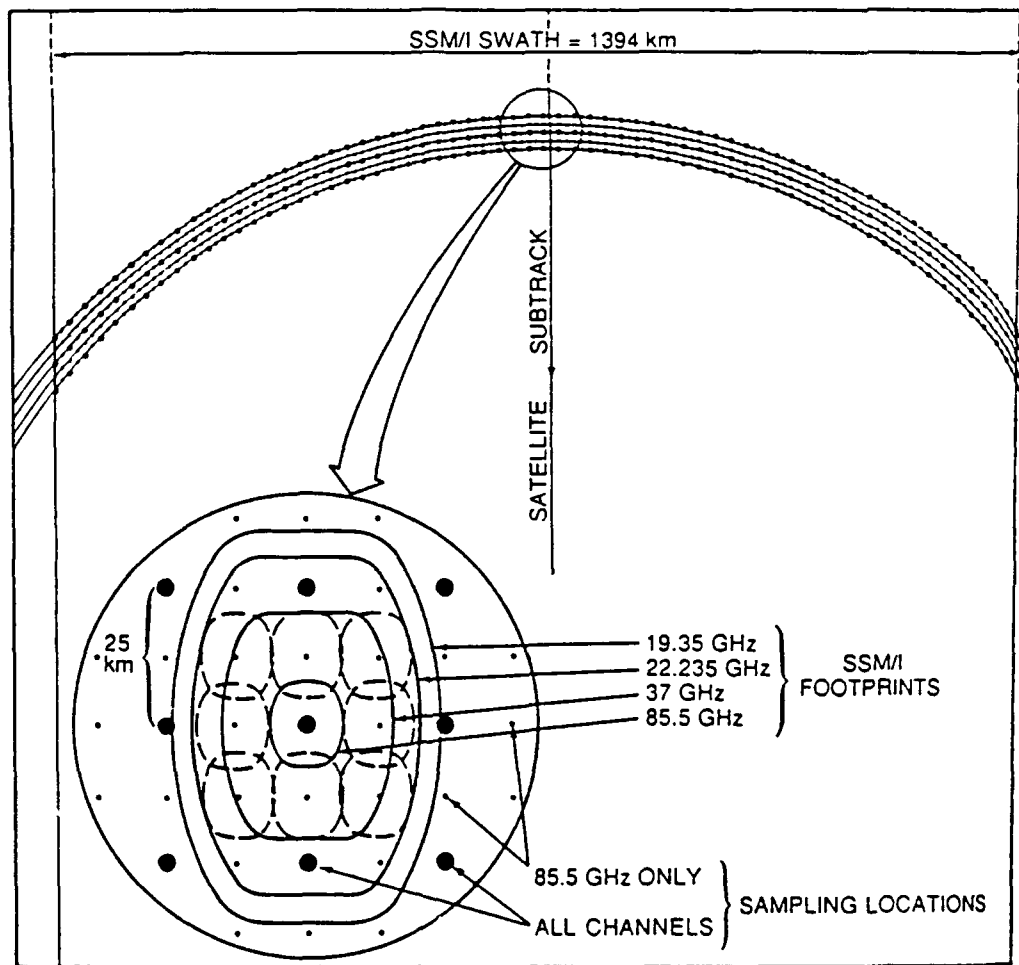
Figure 3.2. Footprints or EFOV of SSM/I channels, and their relationship to scan data points. The heavy dots represent sampling locations common to all channels and they are measured during A scans. From Spencer et al. (1989).

The combination of SSM/I's scan length and F8's orbit produce the pattern illustrated by Fig. 3.3. This pattern is perhaps the most troublesome part of applying SSM/I data to hurricane and typhoon observation. It is necessary to match the sub-satellite track to within about three degrees (333 km) of the vortex center to enable sufficient coverage of the typhoon. Since, as shown in Fig. 3.3, satellite coverage over the tropics is sparse the amount of SSM/I data which were applicable to this study was sparse.
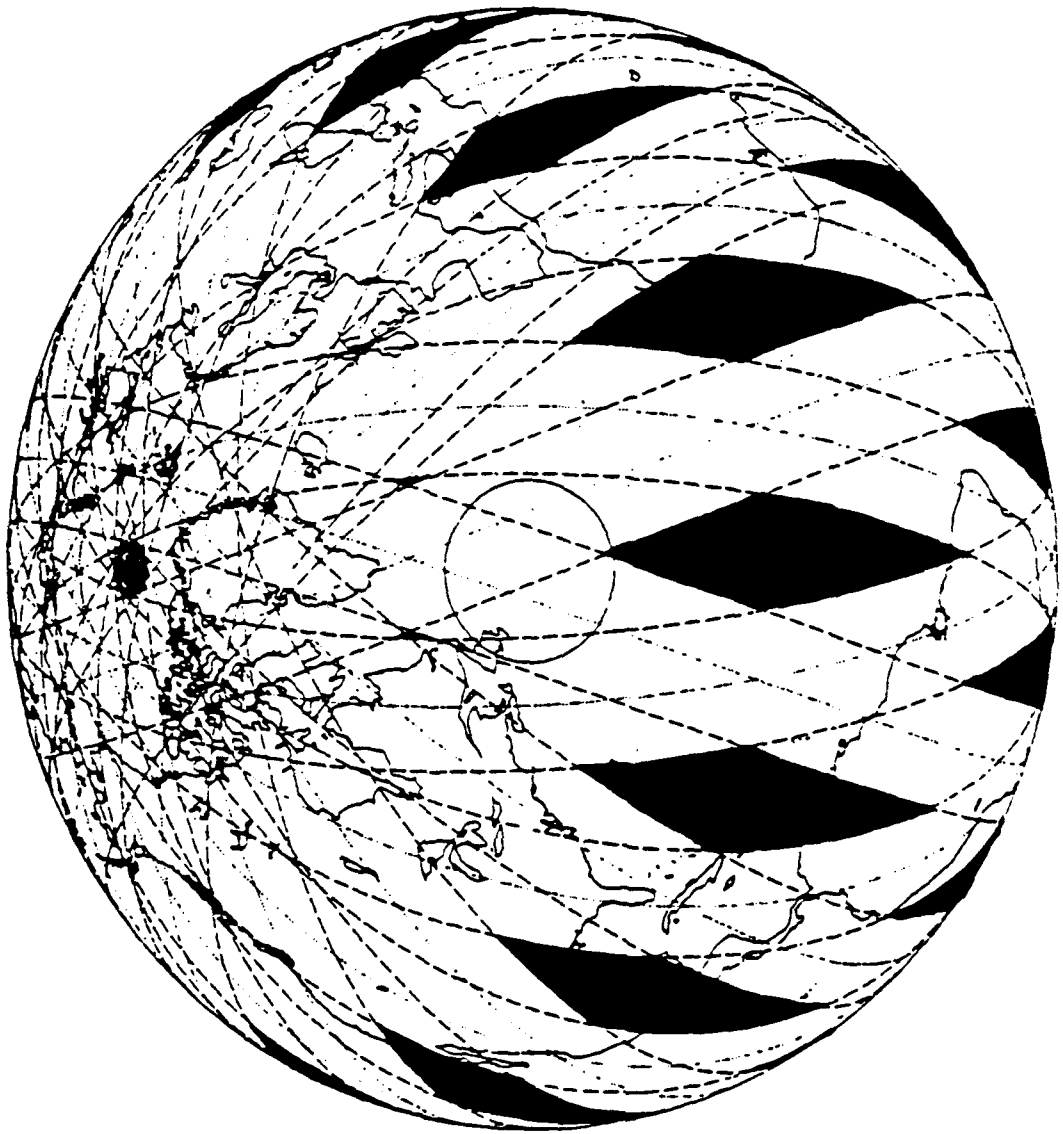
Figure 3.3. Coverage of SSM/I in 24 hours. Due to the
narrowness of SSM/I's scan swath, the tropics have
large data void areas (black regions). From Hollinger
et al. (1987).

16

4. PROCEDURE

a. General

Matching orbits to storms was an important step in the experimental procedure. It required superposition of satellite sub-tracks and typhoon tracks within a common time frame. This was accomplished by plotting 1987 (and Susan, 1988) typhoon storm tracks, as given by the Joint Typhoon Warning Center's (JTWC) fix data, on a Northern Hemispheric polar stereographic chart. Each storm was labeled and its 6-hourly positions marked. A transparent F8 orbit was overlaid on the chart. The transparency depicted the orbit's sub-track, scan arcs, and time-past-ascension hack marks. It was joined to the chart at the North Pole and able to rotate on the face of the chart.

Once the chart and transparency were constructed, a five step operation was performed to determine which orbits contained SSM/I data on typhoons. These steps were:

1) Determine a prospective orbit by comparing orbit date time groups (DTG) with those of the storms. Conway (1989) listed orbital information and the chart provided storm DTG. Once a prospective match was found, step 2 was enacted.

2) Rotate the transparency to the ascension longitude.

3) Compare the satellite sub-track to the storm track. If the storm was not within three degrees latitude of the sub-track at time of passage, skip step 4. Otherwise proceed to step 4.

4) Use the scan arcs, time hacks, and eye locations to get a precise time over storm. This time is important for extracting the SSM/I data from the SDR. A couple of minutes error would result in missing the eye, and possibly missing the storm, since the satellite travels at 6.58 km sec^{-1}.

5) Continue the first four steps until all typhoon DTGs have been checked.

After the storms were matched to SSM/I orbits the SSM/I data was extracted from archives and processed by various programs. The first of these programs mapped the SDR data into a Mercator projection. The second program converted the Brightness Temperatures of the SDR into rainfall rates. The third and last main-frame program was the statistical program "Boxstats" (Felde, 1990).

The Mercator grid was uniformly spaced with a 10 km distance between each point. Since this distance was less than that of the scan points, and since the scans were arced, scan points and grid points seldom coincided. To fill the grid, surrounding data within

the EFOV were interpolated to the grid. Each channel had its own grid. The simpler Mercator projection enabled easier statistical processing of the SDR data.

Perhaps the key to this set of experiments was the second program – the one which converted TB into rainfall rates. This program implemented the non-linear algorithm suggested (Olson et al. 1990) as an improvement over the original linear algorithm used to create the Environmental Data Records' (EDR) rainfall rate. The algorithm is valid for tropical oceanic rainfall only, so care was made to ensure that only oceanic storms were examined. Three filters ensured that fitting data were applied to the proper algorithm formulae. These formulae are:

1) If 85GHz data were available:

$$R = \exp(3.06231 - .0056036 \, TB_{85V} + .029478 \, TB_{85H}$$
$$- .0018119 \, TB_{37V} - .00750 \, TB_{22V}$$
$$+ .0097550 \, TB_{19V}) - 8.0 \text{ mm h}^{-1}. \qquad (5)$$

Where R is rainfall rate in mm h^{-1}.

2) If 85GHz data were unavailable:

$$R = \exp(5.10196 - .05378 \, TB_{37V} + .02766 \, TB_{37H}$$
$$+ .01373 \, TB_{19V}) - 2.0 \text{ mm h}^{-1}. \qquad (6)$$

3)   If R < 0:

$$R = 0. \tag{7}$$

For certain experiments it was necessary to categorize rainfall into convective and stratiform rates. During those experiments the definition of 3 mm h^{-1} was used for initial convective rainfall rate. This relatively low figure was selected with consideration of the area covered by an SSM/I grid point (100 km^2), and is consistent with recent works involving similar scale (Willoughby, 1988).

The third program examined the rainfall rates of a typhoon at map times and performed basic statistical functions on the data within a box of specified half-side (or "radius").   These statistics were maximum, minimum, standard deviation, variance, and frequency distribution of the rainfall.

The box which bounded the data was oriented along the direction of typhoon translation.   Thus the box legs were either parallel or perpendicular to the translation vector. The legs were twice as long as the "radius".   Six radii were used to examine various regions of each typhoon, these were 28, 55.5, 111, 222, 333, and 444 km. Thus the largest box covered an area of 64 square degrees latitude.   Each box was also divided into right and left halves, with the dividing

line coinciding with the translation vector. Figure
4.1 illustrates how the boxes were laid over the storm.

Not all grid points within a box had non-zero
rainfall rates. Further, the statistics of "Boxstats"
ignored zero-data grid points. This produced
statistics that were not true area statistics, which
will be discussed in greater detail later. The
frequency distribution divided the rainfall into
classes which each spanned 2.5 mm h^{-1}; e.g., 0 - 2.5,
2.5 - 5.0, etc. It reported the number of grid points
within the box (or half-box) which had rainfall in each
class.

The statistics from "Boxstats" were joined with
other pertinent information about each map time (e.g.,
DTG, name, orbit, etc.) in a database and processed
further in personal computer spreadsheets. These
processes will be explained in detail later.

It is necessary to define some terms unique to the
experiments in order to properly describe the
experiments. Figure 4.1 helps define one such term -
the annulus. Unlike the normal circular shape defined
as an annulus, this experiment's annuli were square.
It was defined as an outer box minus the next smaller
inner box. For example the 444 km annulus was the area
remaining when the 333 km box was subtracted from the
444 km box. The half annulus is similar but
constructed with half-boxes (right or left).
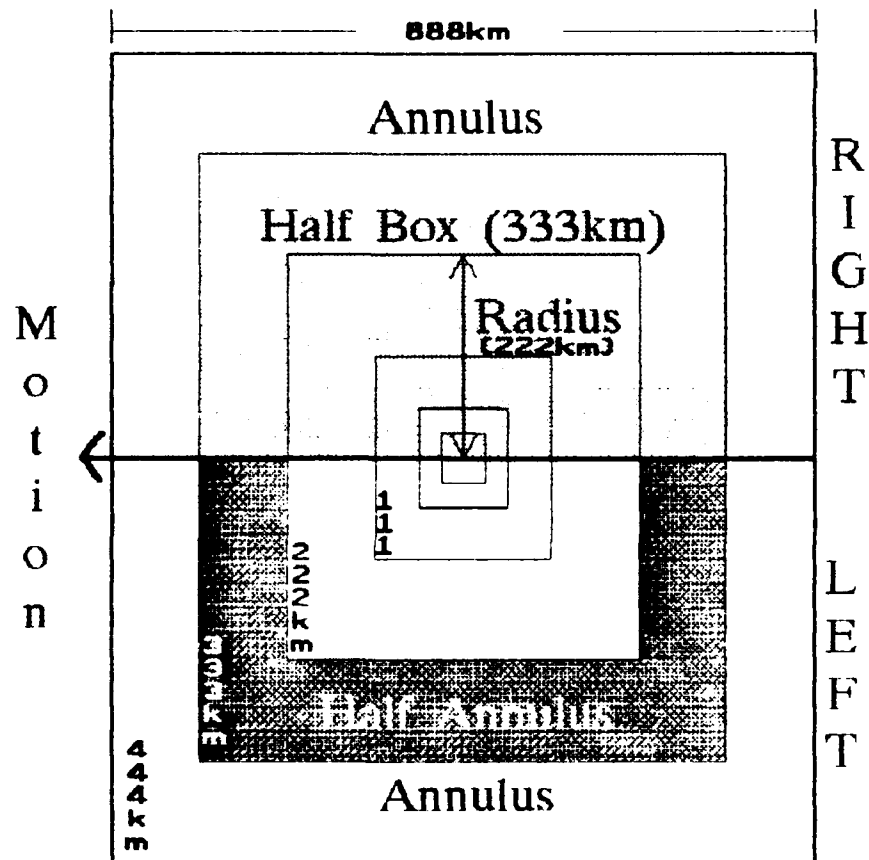
Figure 4.1. Various types of areas used in averaging and totalling rainfall. The line along the direction of motion (x-axis) divides the area into right and left halves. The terms: annulus, box, and radius (equal to the half-side of a square) are illustrated.

Normalized mean rainfall rate was a rate normalized to the area involved (either of an annulus or box, or their halves). This number will very likely differ from the mean rainfall rate since the mean is based on grid points with precipitation but the normalized rainfall is based on the entire area involved. A comparison of the two equations is helpful:

$$\text{Mean R} = (\sum_{i=1}^{n} r_i)/n \qquad (8)$$

$$\text{Normalized R} = (\sum_{i=1}^{n} r_i)/A \qquad (9)$$

Where: R is overall rainfall rate,

r_i is rainfall rate of grid point i,

n is number of precipitation grid points,

A is the total area of the box.

Deepening is an indicator of vortex intensification and is defined as the 24 hour change in central pressure. Its formula is final (24-h) pressure minus initial pressure. Thus a storm with positive deepening is intensifying. The opposite of deepening is filling.

Location and motion data from the Best Track data produced by JTWC and pressure data from the Hong Kong

Royal Observatory (Staff, 1988) were treated as the truth for these experiments.

b. The Experiments

Several experiments were conducted to examine the ties between rainfall distribution and typhoon characteristics. These characteristics were translation speed and direction, central pressure, deepening, and future (24-h) central pressure. Rainfall distribution was examined by use of mean, maximum, and normalized rainfall rates; total, convective, and stratiform rainfall and rainfall rates; and areal comparisons.

Experimental results were judged good if a strong (i.e., greater than .5) linear correlation existed. By this standard several experiments failed. Notably, no good correlation was found between storm translation speed and any of the rainfall distribution schemes listed. Also, no strong correlation was found between rainfall asymmetries (left vs right boxes) and any storm characteristics. Five experiments were successful though, and are listed below.

b1. Mean Annular Rainfall Rate vs. Deepening

Mean annular rainfall rate was calculated using the formula:

$$\bar{R} = (\bar{R}_o N_o - \bar{R}_i N_i)/(N_o - N_i) \qquad (10)$$

Where: $\bar{R}$ is mean annular rainfall rate,

o designates outer box values,

i designates inner box values,

N is the total number of precipitation grid points.

This value was calculated for each annulus of every storm. The storms were organized in order of increasing deepening. Finally, each storm's rainfall rates were examined to determine which were local maxima; these are listed in **bold** type in Table 4.1.

b2. Case Studies

Two typhoons, Lynn (1987) and Dinah (1987), had sufficient map times (seven and four, respectively) to enable a study of their life cycles. Total rainfall for all box sizes was computed and compared against the future (24-h) central pressure of the typhoons. In addition, as a means of comparison, the same treatment was done for all storms.

Table 4.1. Mean rainfall rates (mm h^{-1}) for various orbits (each orbit signifying a pass over a typhoon) and for annuli of different sizes. Note that negative deepening represents filling.

Deepening (mb/day)	Orbit	Annuli					
		28km	55.5km	111km	222km	333km	444km
-23	4912	3.05	3.65	3.96	2.49	1.63	1.70
-22	1007	2.17	2.23	2.77	3.05	2.40	1.92
-20	1161	2.86	2.21	3.13	2.91	2.22	1.63
-20	1791	1.47	3.44	2.17	1.60	1.25	1.27
-19	513	1.99	1.66	1.64	2.08	1.71	1.46
-14	1000	2.39	2.81	2.31	2.62	2.08	1.48
-10	428	2.74	2.00	1.09	0.67	0.55	0.80
-10	1748	3.73	3.85	4.54	3.00	1.99	?
-9	1805	0.92	1.06	1.27	0.85	0.90	1.21
-8	1176	1.74	1.57	1.86	2.34	1.87	1.54
-7	1798	1.82	1.76	2.06	1.59	1.30	1.41
-7	1812	0.49	0.56	0.60	0.79	1.24	1.53
-2.5	1416	2.14	2.43	2.73	1.92	1.13	0.93
1	505	4.88	3.82	2.56	1.50	1.14	0.98
2	506	1.61	1.68	2.37	2.10	2.03	1.80
2.5	2200	2.14	2.73	2.54	1.79	1.56	1.36
5	788	2.77	2.37	1.84	1.62	1.40	1.25
7	1621	2.30	2.60	3.01	2.36	1.84	1.52
7.5	1635	1.81	2.36	2.21	2.23	1.60	1.17
10	1642	2.16	2.73	2.64	2.32	1.54	1.11
10.5	1105	3.86	3.51	2.44	1.55	1.44	1.27
15	1691	2.85	2.67	2.57	2.45	2.04	1.52
17	1698	2.74	2.97	3.22	2.36	1.55	1.17
22	1147	3.43	3.16	3.13	2.71	1.86	1.29
30	936	5.22	4.93	3.78	2.18	1.51	1.20
32	1104	2.91	2.59	1.94	0.97	0.70	0.68
40	929	2.41	3.47	3.57	2.81	1.54	1.12

Figure 4.2 plots Lynn's path, and Figure 4.3 does the same with Dinah. Points on the paths correspond to map times and indicate the DTG along with translation and strength data.

b3. Cross-sectional Studies

Normalized annular rainfall was computed for each half annulus for all storms, and plotted against distance from eye. As way of convention, left annuli were treated as negative (and therefore on the left side of the origin, on the number line) and right as positive. This gives a pseudo-cross-sectional view of each storm. It isn't a true cross-section since the plot represents statistical halves -- not a true slice through some portion of the storm. Storms were stratified into four classes: rapidly filling or storms with -10 or less mb/day deepening; moderately filling or -0 to -9 mb/day deepening; moderately deepening with 0 to 9 mb/day deepening; and rapidly deepening with 10 or more mb/day deepening. A class composite was calculated by computing the class average of each half annulus.

b4. Precipitation Intensity Parameter

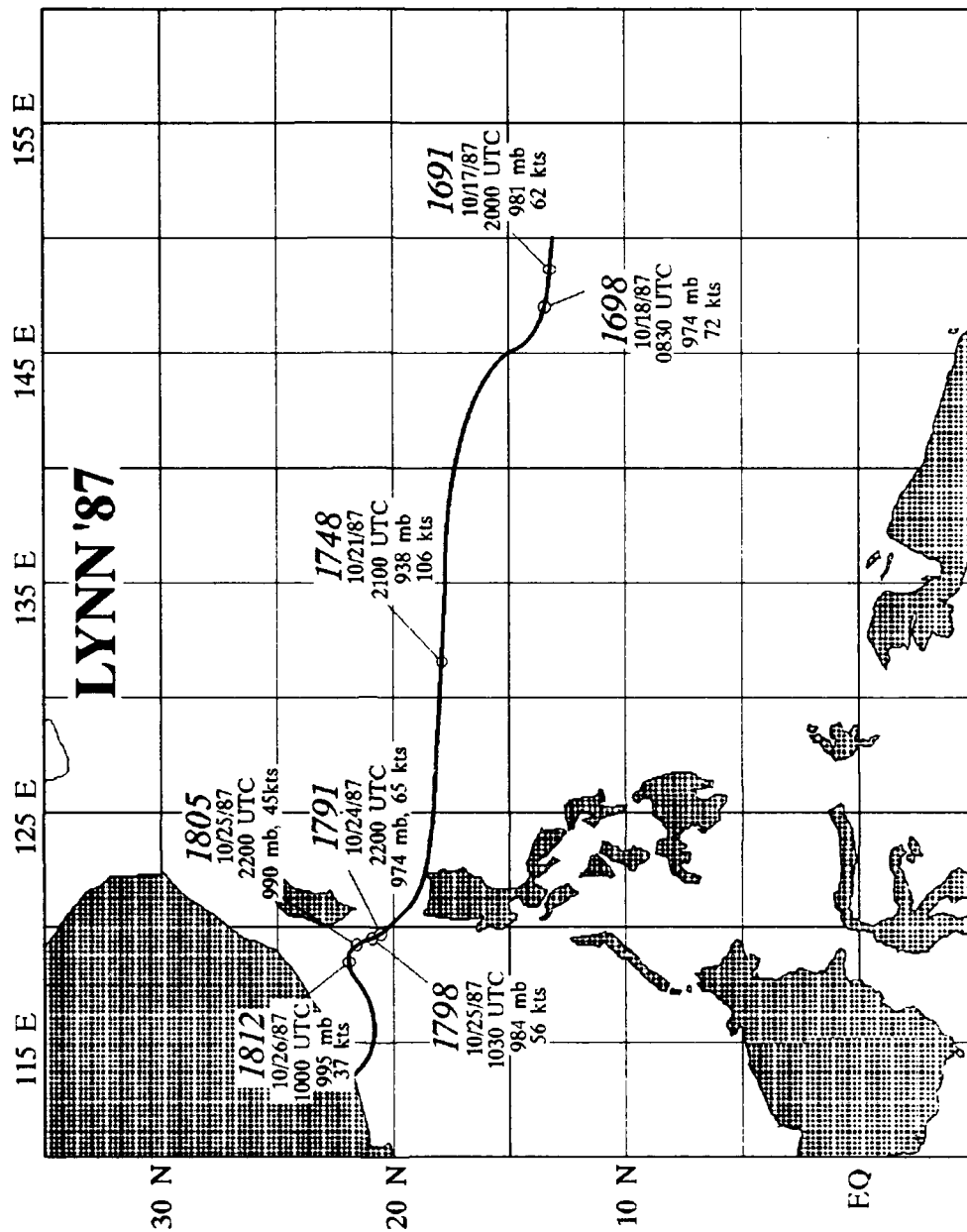Figure 5.1. Rainfall rates within 28 and 222 km boxes of Typhoon Lynn (1987) and 24-h central pressure as a function of time. Linear fit data: for 28 km boxes, $P = -2.86R + 1012.5$; for 222 km boxes, $P = -.07R + 1021.1$; R is in units [$mm^3 \ h^{-1} \times 10^{14}$] Note the negative correlation between rainfall rates and 24-h pressures of Lynn.
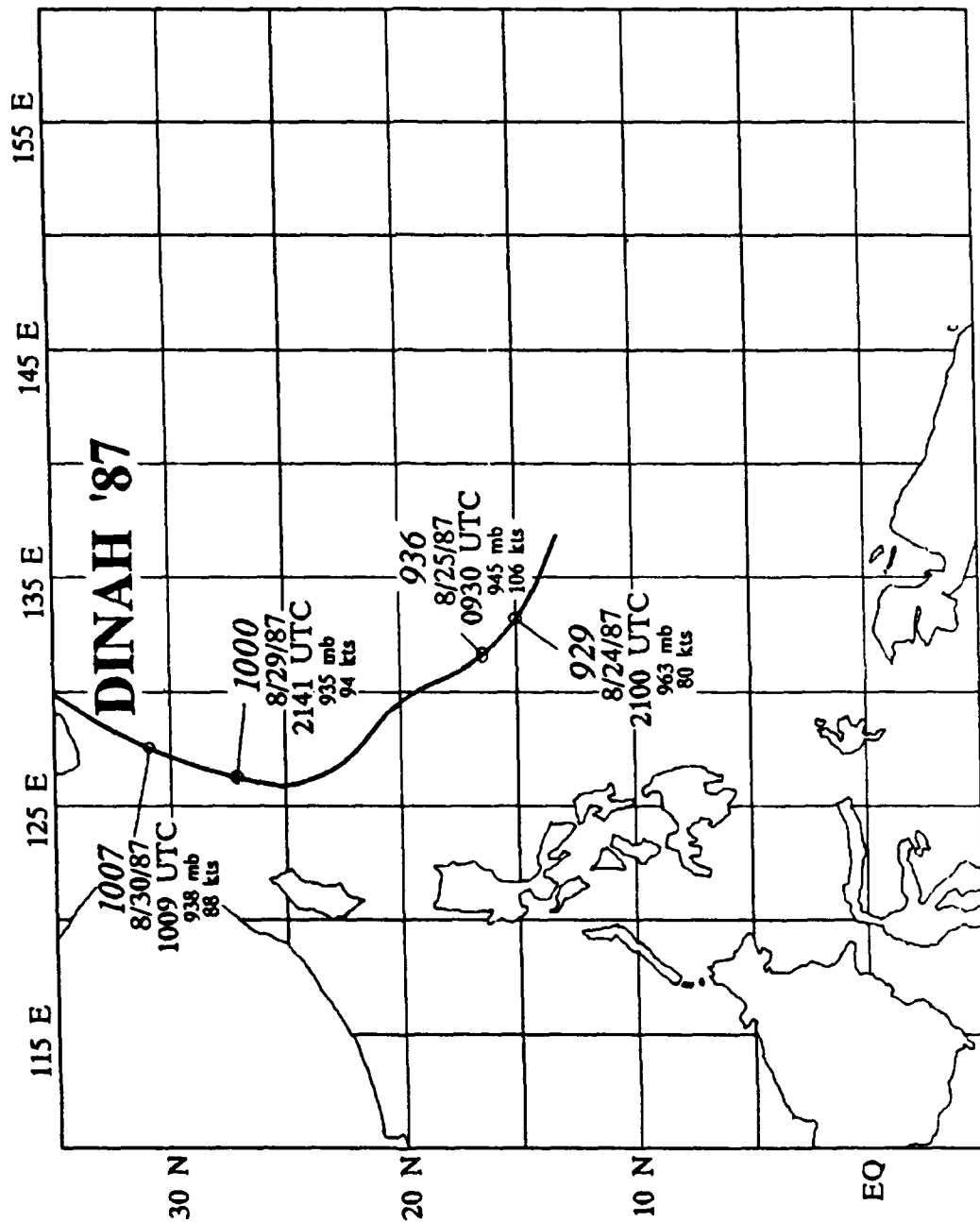
Figure 4.3. As in Fig. 4.2 except of Super Typhoon Dinah's (1987) Best Track.

A measure of the convectve contribution to the overall rainfall is the precipitation intensity parameter (PIP). The PIP is the ratio of convective rainfall divided by the total rainfall expressed as a percentage, or PIP = $R_c/(R_c + R_s)$ x 100% where the subscripts denote convective (c) and stratiform (s). PIPs were calculated for a variety of box and annular sizes. The PIPs were then compared to storm deepening and 24-h central pressure.

b5. Northwesterly Moving Storms

When the sample storms were stratified by translation characteristics (see Fig. 4.4 and Fig. 4.5) it became clear that a large proportion of the storms were northwesterly movers. Northwesterly movers were then examined to see if they behaved in a maner that was more predictable than the entire sample set. A series of stratifications were constructed to complete this examination. These rates were: a) mean stratiform rainfall, b) total stratiform rainfall, c) mean convective rainfall, d) total convective rainfall, e) mean total (convective and stratiform) rainfall, and f) total combined rainfall.

DIRECTION

Figure 4.4. Pie chart of typhoon map time distribution by translation direction. Note the large proportion of northwesterly movers.

SPEED

> 12 Kts
22.2%

1 – 6 Kts
37.0%

7 – 12 Kts
40.8%

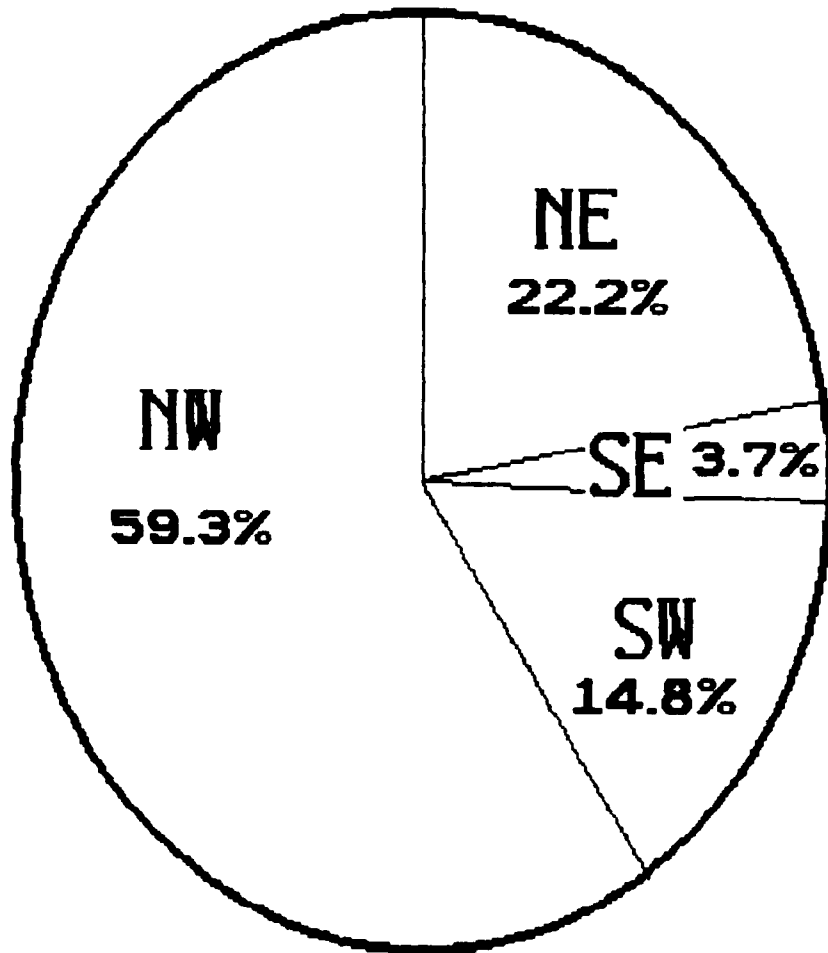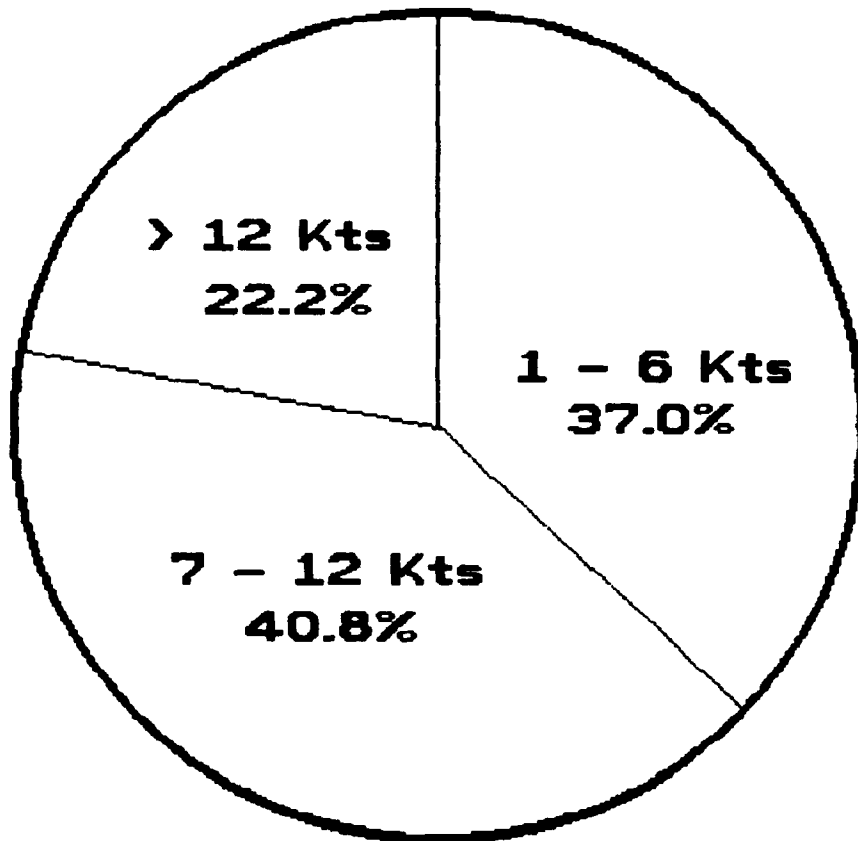Figure 4.5. Pie chart of typhoon map time distribution by translation speed.

5. RESULTS

a. Mean Annular Rainfall Rate vs. Intensification.

Table 4.1 lists the 27 map times in order of increasing intensification (deepening), with 929 being the most rapidly deepening map time showing a 40 mb/day pressure change. The mean annular rainfall rates are given for each storm and map time, with the local maxima printed boldly. The only deepening storm to have a multiple peak (Kelly 1987, orbit 1635), actually had a very weak second peak, almost a plateau. Thus a pattern of single and multiple peaks emerges from Table 4.1, and is tabulated in Table 5.1. In all but one case (90% of the time) multiple local maxima were associated with filling storms and in 13 of 16 cases (81%) single peaks were associated with deepening storms. The lower portion of Table 5.1 gives greater detail by presenting a frequency distribution. It illustrates that rapidly deepening storms always had single peaks and rapidly filling storms nearly always (86%) had multiple peaks.

The peaks represent regions of intense precipitation perhaps due to rainbands. Because of our procedure these regions are annuli. In a single-peaked storm the rainband (in most cases within 111 km of the center) supports the vortex's central pressure and

Table 5.1. Frequency distribution of normalized rainfall peaks verses 24-h Delta P (= P_I - P_F, values in mb).

Mode ->	Single Peak	Multiple Peaks
Filling P<0	3	9
Deepening P>0	13	1
-10	1	6
-9 to 0	2	3
0 to 9	5	1
10	8	0

consequently the vortex deepens. In two of the three single peaked cases where the vortex failed to deepen (orbits 1007 and 1812), the infered rainbands were perhaps located 222 and 444 km from the center respectively. Apparently these distances were too far from the core to aid the intensification process. The third case (orbit 1416) involved a slight filling, which was probably due to unknown external influences.

The multiply peaked storms developed two regions of heavy rainfall. These two regions competed for moisture. The result was the creation of a barrier by the outer band effectively preventing the high energy theta-e air to flow into the band closer to the center (see the boundary layer studies by Powell (1990) of hurricanes Josephine (1984) and Earl (1986)). As a result of this competition neither band became as vigorous as it would have been in the absence of the other. The result was a diffused region of latent heat release which could not sustain a deep vortex.

b. Case Studies

Fig. 5.1 depicts the life cycle of typhoon Lynn (1987). Future 24-h central pressure decreased gradually from about 10/17/87 20 UTC to 10/21/87 21 UTC and then rapidly rose. In inverse proportion (r=-.97 and -.96 respectively) to the pressure, the rainfall
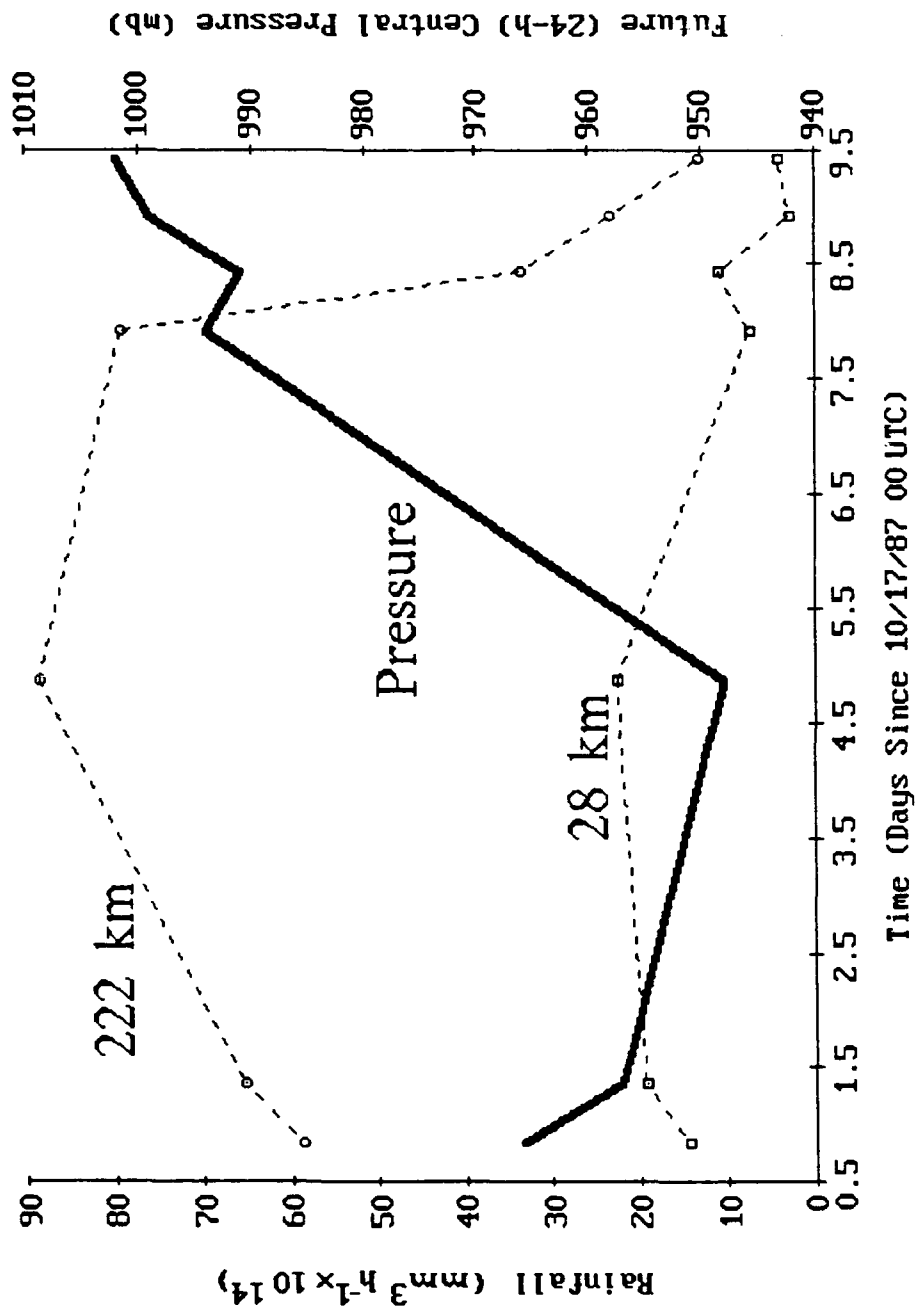
Figure 5.1. Rainfall rates within 28 and 222 km boxes of Typhoon Lynn (1987) and 24-h central pressure as a function of time. Linear fit data: for 28 km boxes, P = -2.86R + 1012.5; for 222 km boxes, P = -.07R + 1021.1; R is in units [mm³ h⁻¹ x 10¹⁴]. Note the negative correlation between rainfall rates and 24-h pressures of Lynn.

37

rates measured in the 28 and 222 km boxes rose and fell. The rainrate measured in other boxes behaved similarly, but with somewhat less correlation (the worst, 444km, had an r of -.52).

Fig. 5.2 illustrates typhoon Dinah's (1987) life cycle as well as the rainfall rates of different box sizes. These rates in the 55.5 km box are inversely correlated (r=-.99) to the 24-h central pressure, and, although not shown, rainfall rates of boxes up to 222 km are similarly inversely correlated. Fig. 5.2 shows the rainfall rates in the 333 km box are positively correlated (r=.99) to the 24-h pressure however. The 222 km rate (not shown) was poorly correlated (r=.22) to the pressure indicating a transition from negative correlations to positive correlations. Caution is advised against generalizing the results because of the small sample sizes.

The transition 'radius' for a typhoon (e.g., 222 km for Dinah) divides the storm into an inner and outer region each with distinct relationships between rainfall and intensity changes. Within the inner region the latent heat release drives down the central pressure (Burpee and Black, 1989). From our analysis there appears to be a 24-h lag between rainfall and the resulting pressure fall. This is similar to the lag observed between convective bursts and increased maximum winds in hurricanes (Steranka et al., 1986).

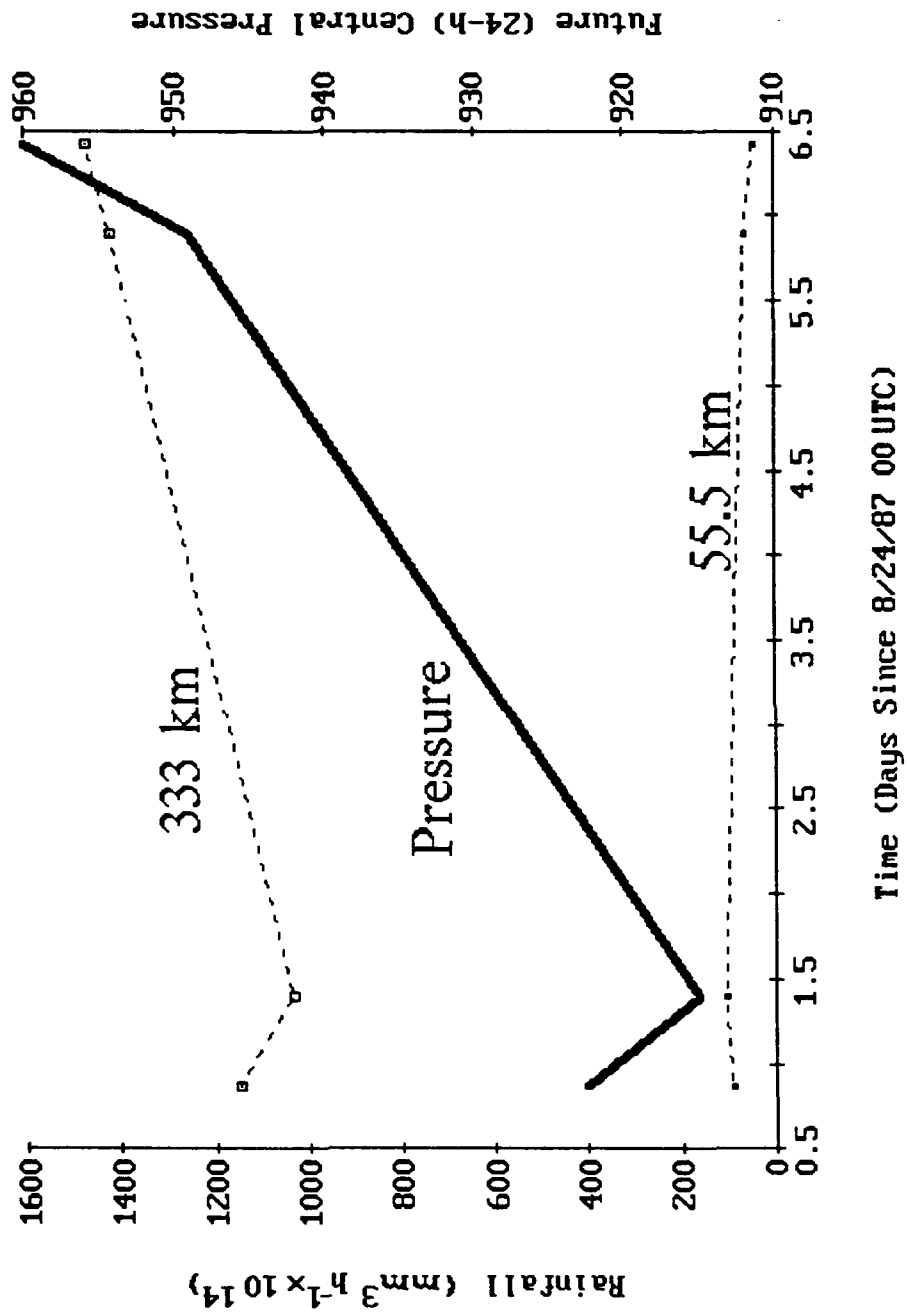Figure 5.2. Rainfall rates within 55.5 and 333 km boxes of Typhoon Dinah (1987) and 24-h central pressure as a function of time. Linear fit data: for 55.5 km boxes, P = -.75R + 990.0; for 333 km boxes, P [mb] = .1R + 800.9; R is in units [mm³ h⁻¹ x 10¹⁴]. Note the possitive correlation between rainfall rate and 24-h pressure at 333 km. This demonstrates the changed nature of latent heat release in the outer region.

38

In the outer region the latent heat release plays an important but opposite role. Since the heat is released further from the core, the thermal effects are spread out. Also, the increased rainfall in the outer region implies the location of a strong rainband. As shown in the bimodal rainfall section, this band cuts off the necessary moisture to maintain the inner convection. Thus the rainfall outside the transition radius results in vortex filling.

This transition radius, or effective radius, varies from storm to storm. It appears to have been between 333 and 444 km for Lynn, and 222 km for Dinah. Previous work based on conventional wind analyses suggested that an effective radius lies between 200 and 400 km (Holland, 1983). Fig. 5.3 shows the rainfall rate in the 222 km box for 26 map times (see Table 5.2) as they related to the future central pressure. The correlation of this least squares fit (r=-.62) was the best of all box sizes. Unlike Dinah, all boxes showed a negative correlation between 24-h pressure and rainfall rates. Overall, due to the best fit at 222 km for all storms, the effective radius appeared to lie just beyond 222 km.
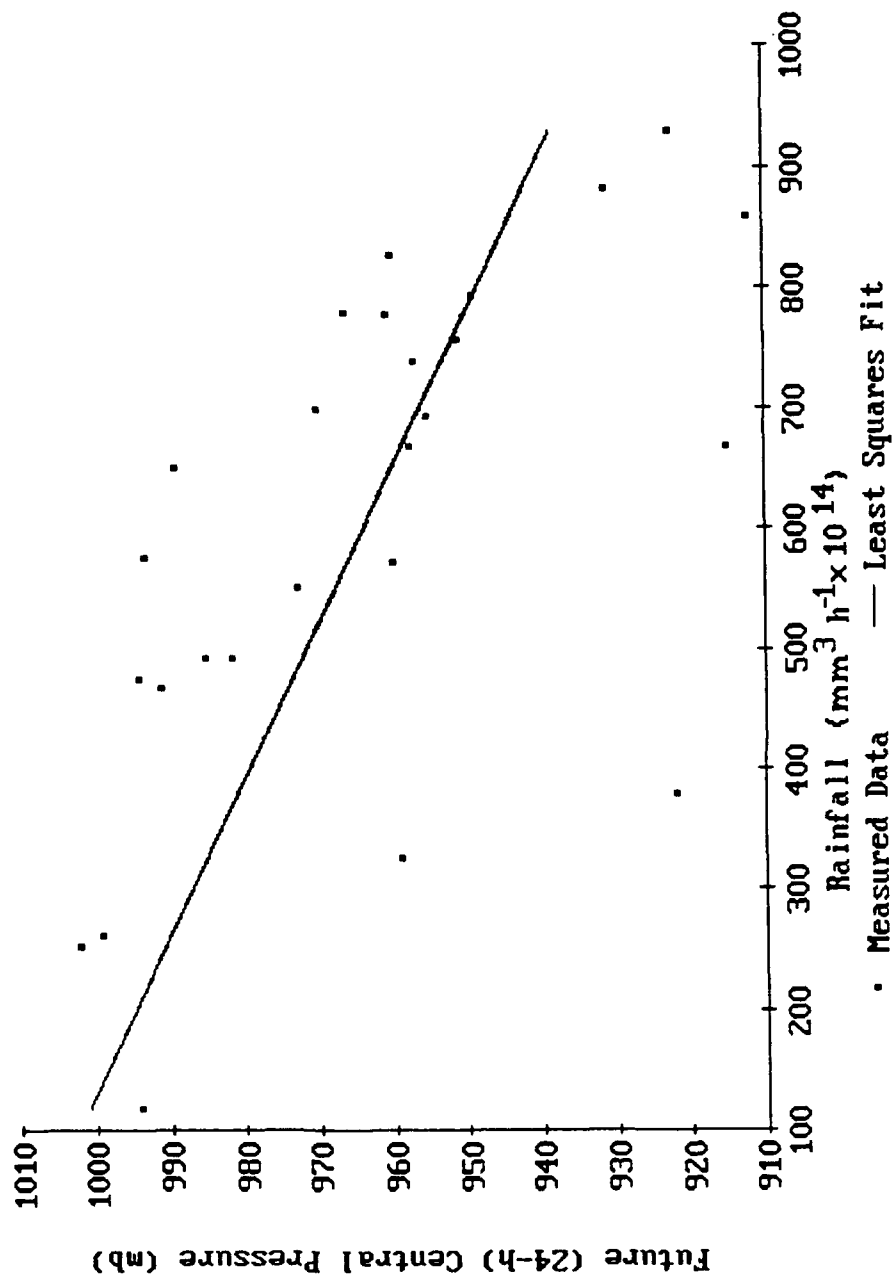
c. Cross-Sections

Figure 5.3. Scatter diagram of rainfall rates within 222 km boxes as a function of 24-h central pressure. Data is from 26 map times of 1987-88 typhoons. Linear fit data: $P = -.077R + 1010$; R is in units [mm^3 h^{-1} x 10^{14}]. Note the negative correlation between rainfall rates and 24-h pressures.

Table 5.2. Typhoons and map times used in the research. Data are in same units as found in text; "ff" is maximum sustained wind (kts). Key to notes:
L - Partially over land.
I - Incomplete data (outer data missing).
NW - Used in northwest movers experiment.

Identification				Characteristics				Motion		
Orbit	Name	Date	UTC	Deep, mb/day	24-h, mb	P, mb	ff, kts	Dir, deg	Spd, kts	Notes
428	Vernon	7/20/87	1000	-10	994	984	57	322	11	NW L
505	Wynne	7/25/87	2030	1	922	923	117	292	15	NW
506	Alex	7/25/87	2200	2	970	972	65	300	11	NW
513	Alex	7/26/87	1030	-19	989	970	65	355	12	NW
788	Cary	8/14/87	2115	5	985	990	63	255	4	
929	Dinah	8/24/87	2100	40	922.5	962.5	80	308	10	NW
936	Dinah	8/25/87	930	30	915	945	106	318	10	NW
1000	Dinah	8/29/87	2141	-14	949	935	94	3	15	
1007	Dinah	8/30/87	1009	-22	960	938	88	22	18	
1104	Holly	9/6/87	700	32	959	991	24	284	9	NW
1105	Freda	9/6/87	900	10.5	981.5	992	57.5	75	2.5	
1147	Holly	9/9/87	800	22	912	934	102	300	3	NW
1161	Holly	9/10/87	800	-20	931	911	64	78	6	
1176	Freda	9/11/87	930	-8	951	943	137	46	4	
1416	Ian	9/28/87	930	-2.5	972.5	970	72	95	1	
1621	Kelly	10/12/87	2100	7	960.5	967.5	75	341	7	NW
1635	Kelly	10/13/87	2050	7.5	957.5	965	80	342	11	NW
1642	Kelly	10/14/87	930	10	955	965	83	320	11	NW
1691	Lynn	10/17/87	2000	15	966	981	62	286	12	NW
1698	Lynn	10/18/87	830	17	957	974	72	301	10	NW
1748	Lynn	10/21/87	2100	-10	948	938	106	255	15	I
1791	Lynn	10/24/87	2200	-20	994	974	65	313	4	NW
1798	Lynn	10/25/87	1030	-7	991	984	56	350	2	NW L
1805	Lynn	10/25/87	2200	-9	999	990	45	253	2	L
1812	Lynn	10/26/87	1000	-7	1002	995	37	273	3	NW
2200	Nina	11/22/87	2100	2.5	960	962.5	83	260	16	
4912	Susan	6/1/88	2230	-23	993	970	71	63	14	L

Figs. 5.4 and 5.5 are cross-sectional views of rainfall within typhoons in various stages of intensification. The cross-section is not a cut through the storm in any particular direction, but represents the statistical right and left halves at various radii.

Fig. 5.4 shows the distribution of convective rainfall within four classes of typhoons: a) rapidly filling, b) moderately filling, c) moderately deepening, and d) rapidly deepening. In general, the following points are noteworthy:

1) The peak volumetric rainfall rate increases as deepening increases. This generality has an exception since the rapidly filling storm's composite reaches a peak of about 20 (mm^3 h^{-1} x 10^{14}) which is greater than the moderately filling composite. This exception arose because of typhoon Susan (1988, orbit 4912) which had an extraordinary effect on the composite. Susan's data were contaminated by land as she made landfall over Taiwan.

2) As the composite storm intensifies, the convective rain becomes more core intensive. That is, proportionately, more of the area under the composite plot is within one degree of the eye. As filling increases, the composite plot becomes flatter.

3) As the composite storm intensifies, the total area under the composite plot increases. This suggests
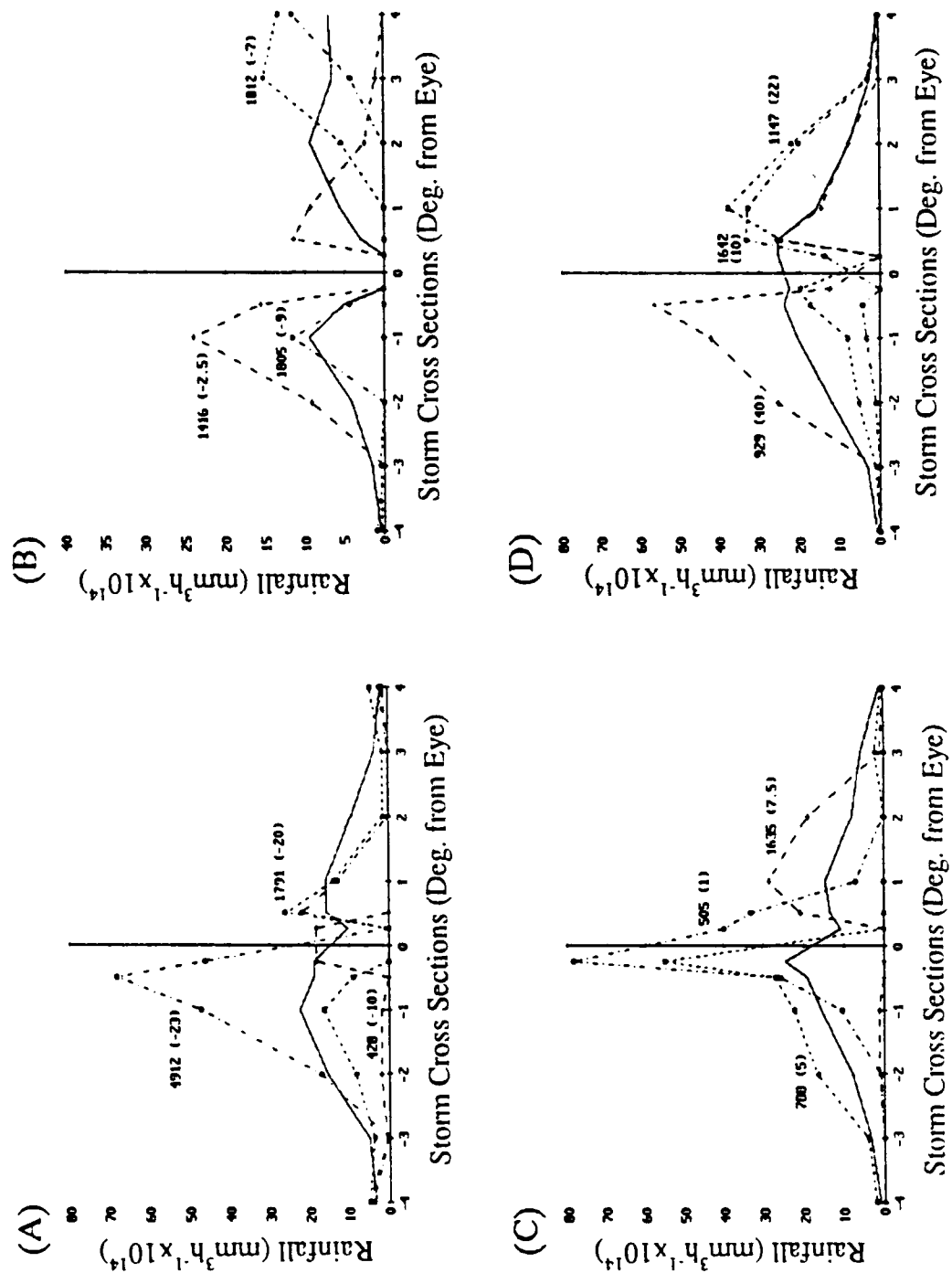
Figure 5.4. Cross-sections of convective rainfall of four typhoon (1987-88) classes: a) Rapidly filling (>10 mb/day) storms, b) Moderately filling (0 to 9 mb/day) storms, c) Moderately deepening (0 to 9 mb/day) storms, and d) Rapidly deepening (>10 mb/day) storms. Orbit numbers label three storms within each class, numbers in brackets are deepening [mb/day]. Solid line represents the class composite. In general, the composite line becomes more peaked as the storms intensify.
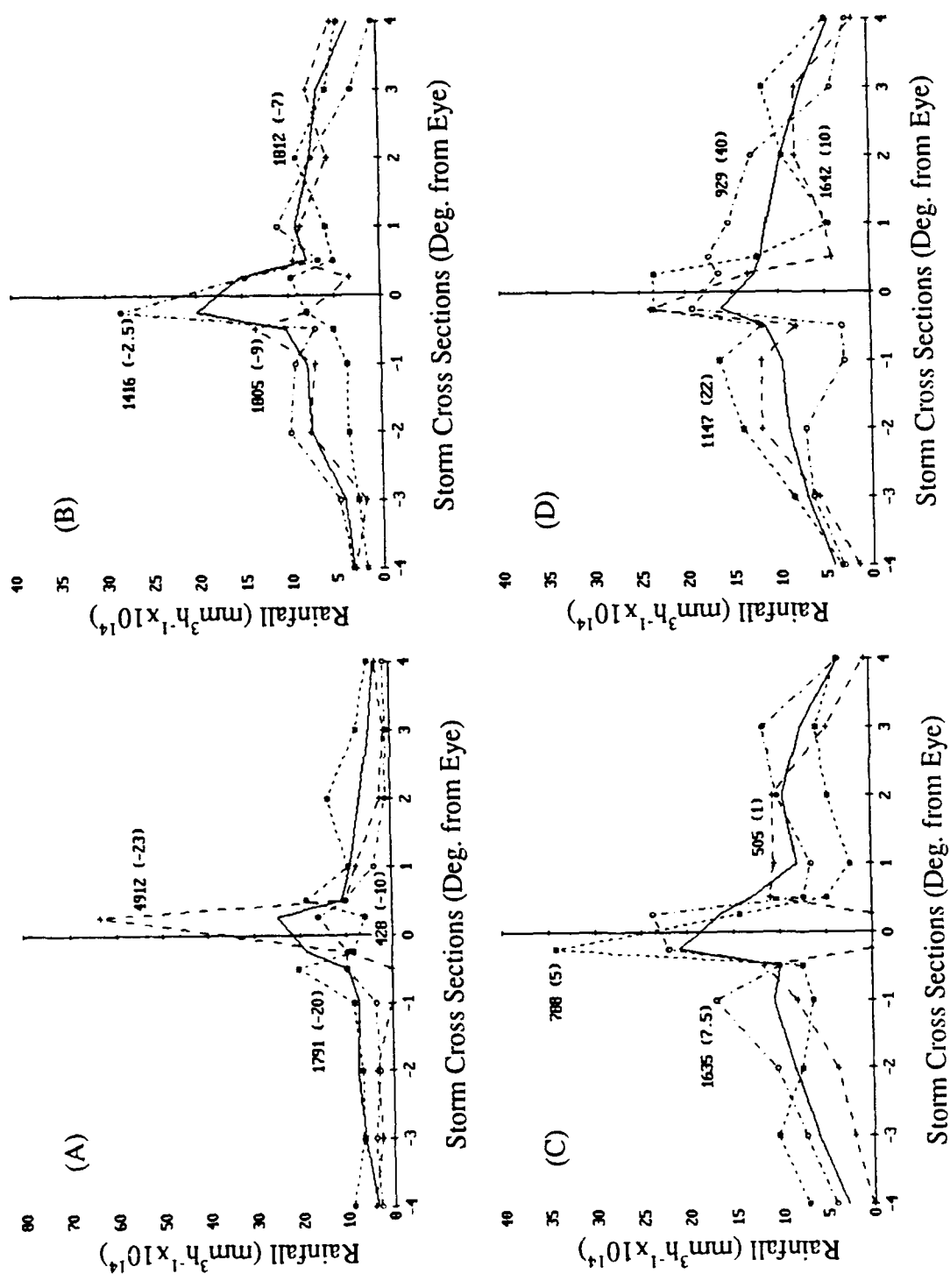
43

Figure 5.5. As in 5.4 except for stratiform rainfall.
Note that the area under the composite increases with
intensification.

44

that as total convective rainfall increases the storm deepens.

Similarly, Fig. 5.5 shows the distribution of stratiform rainfall. In general, two observations can be made when comparing the class composites:

1) As deepening increases in magnitude the composite plot becomes less peaked. The spikes appear to have had broader bases as a storm deepened.

2) As the composite storm deepened the area under the composite plot increased revealing that total stratiform rainfall had increased.

When compared to the convective patterns in Fig. 5.4, the stratiform rainfall patterns appear to be flatter and more uniform. This uniformity suggests that the stratiform pattern may be the better forecasting tool. However, the stratiform signatures are subtle, and may be difficult to recognize in practice.

These results illustrate the kind and amount of precipitation of typhoons in various stages of their maturation. As rainfall increases latent heat is released at greater rates and the vortex deepens. This is consistent with observations (Willoughby, 1988). A compounding effect is the trend for convection to become core intensive as a storm develops. This provides an efficient "focus" of the energy, affecting the central pressure directly.

As convection flattens away from the core, the storm looses some of its "focus" and its central pressure rises. It is not clear if this is a cause or an effect of overall reduced precipitation, but both are associated with a typhoon's demise.

d. PIP

Fig. 5.6 illustrates how PIP of the 444 km box is related to typhoon deepening. As storms deepen, their overall (i.e., largest box) PIP decreases, that is, the relative convective contribution to the the storm's rainfall decreases. Conversely, as a storm decays, its relative convective activity increases.

While the correlation coefficient (r=-.55) is not as strong as those in other experiments, the trend does help define what was observed in the cross-sections. The trend of convection to increase with deepening is not as strong as that of stratiform rain to increase with deepening. This is not surprising since the cross-sectional view represented area-normalized rainfall rates. The rise in convective rates with deepening is largely in the core, where the area is much less than the outer region's area. Since stratiform rainfall rates increase more uniformly throughout the storm as deepening increases, total non-convective rainfall increases more rapidly than the
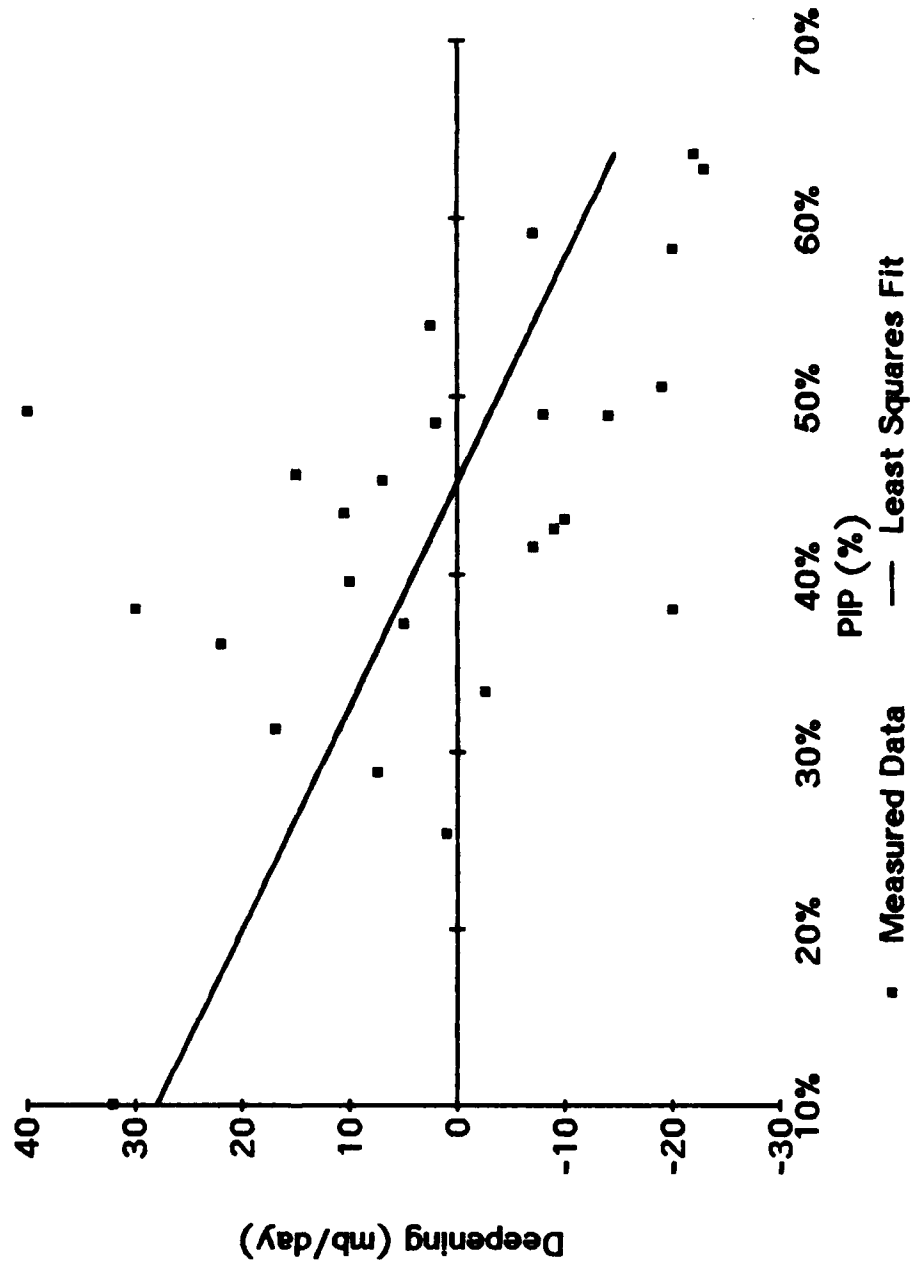
Figure 5.6. Scatter diagram of typhoon deepening as a function of the Precipitation Intensity Parameter (PIP = convection/ total rainfall x 100%) within 444 km boxes. Minus deepening represents filling. Linear fit data: D = -79.6PIP + 36; PIP in percentage, D in units [mb/day]. Note that as storms fill they become more convective.

total convective rainfall. Thus PIP should (and does) decrease with increasing intensification.

There is also a tie between this finding and bimodal characteristics. A second rainband would clearly increase overall PIP and has already been linked to typhoon filling.

Fig. 5.7 is the first of two scatter diagrams which relate PIP to future central pressure. It depicts the PIP of 444 km annuli, and projects a least squares fit (r=.59) on the data. As convection in the outer regions become the dominant form of rainfall (as shown by higher PIPs), the storm decays. This is consistent with the overall finding in Fig. 5.6 and the observations made about multiply peaked storms. Strong convection relative to stratiform rainfall in the 333 - 444 km annulus is a sign of a weak typhoon.

Fig. 5.8 shows how the inner PIP correlates positively to strong typhoons. The PIPs of right half-annuli from 28 - 55.5 km are correlated with future (24-h) central pressure. This annulus yielded the strongest correlation (r=-.55). Generally the right annulus PIP correlated better than the left. It is probably related to the vortex's motion, since the right side of a moving cyclone develops stronger winds and convection.

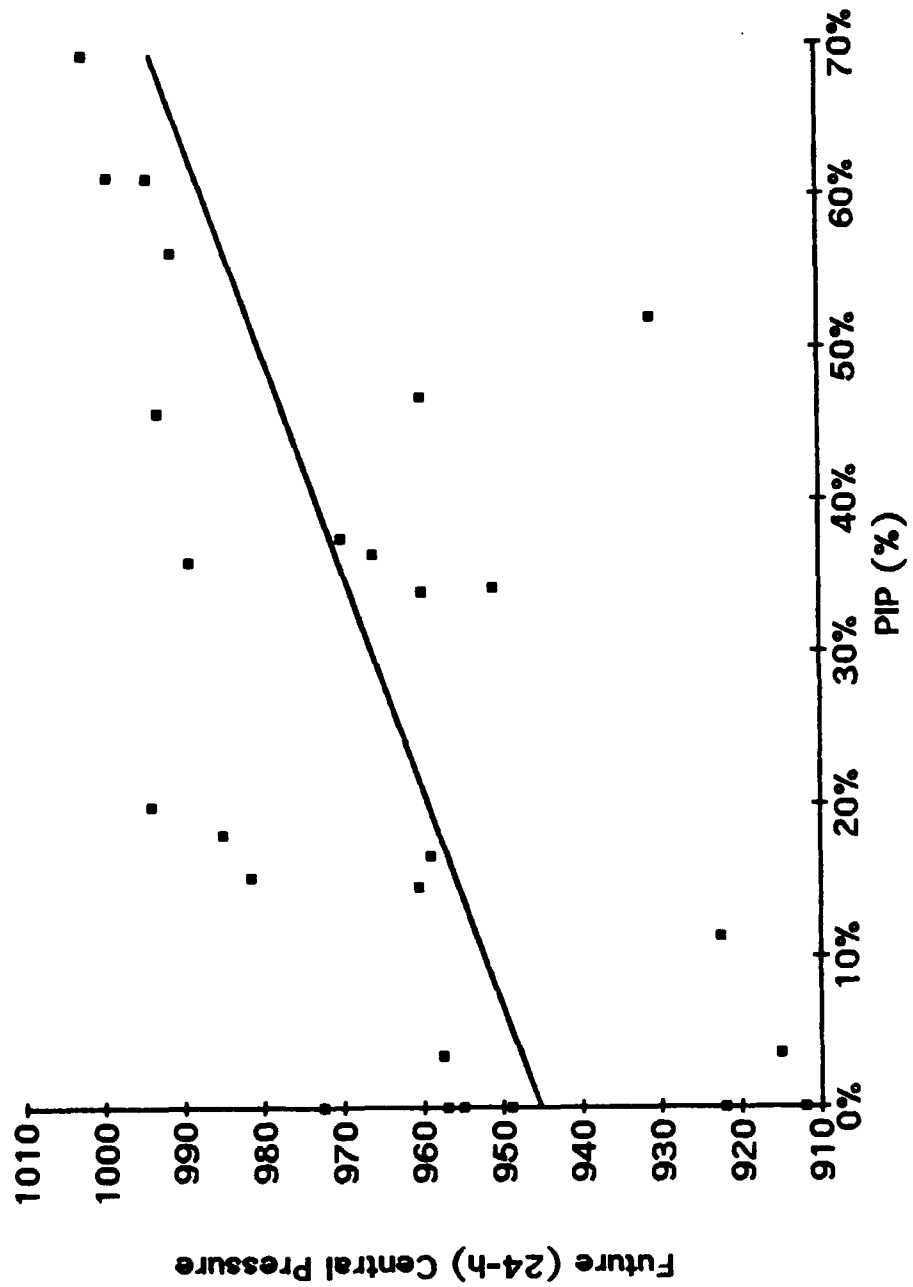The effect of strong convection in the inner region clearly is to lower the central pressure. This,

Figure 5.7. Scatter diagram of 24-h central pressure as a function of PIP within the 333 to 444 km annulus. Linear fit data: P = 69.5PIP + 945.4; PIP in percentage, D in units [mb/day]. Note that the convective portion of storms increase as they weaken.
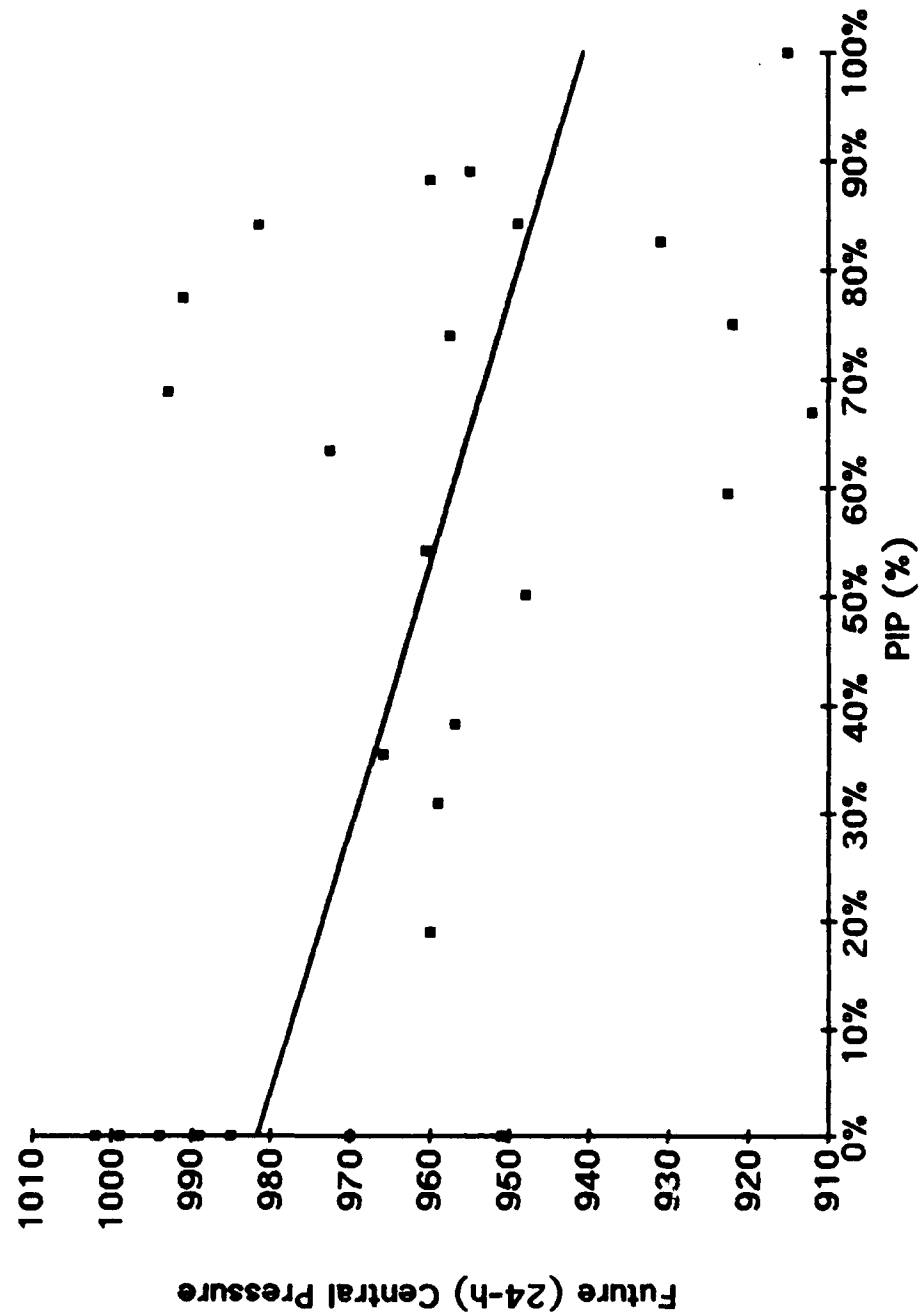
Figure 5.8.   As in 5.7 except PIP is computed in the 28 to 55.5 km right half-annulus.   Linear fit data: P = – 40.9PIP – 981.6;   PIP in percentage.   Convective dominance in the innermost regions is associated with vigorous storms.

too, has been previously discussed. The core PIP rises because the central convective peaking surpasses the rise in stratiform precipitation in deepening storms.

e. Northwest Movers

Figs. 5.9 and 5.10 illustrate the effects of stratiform rainfall rates on storms which were moving in a northwesterly direction. The stratiform rainfall rates were measured within 111 kms of the eye and thus represent the inner region. While the correlation of the data to least squares fit (r=.75 and r=-.78 for Figs 5.9 and 5.10, respectively) was best at 111 km, good fits also occurred within the 55.5 and the 222 km boxes. Also, data correlated better against 24-hour central pressure than against deepening in all the boxes mentioned.

Figs. 5.11 and 5.12 show the effects of convective rainfall on future pressure. Fig. 5.11 is a scatter diagram of future pressure as a function of mean convective rainrates in the 28 km box. Due to the definition of convective rain there are no data between 0 and 3 mm/h. The figure shows the rate of core convection has a significant role in 24 hour pressure development. Fig. 5.12 depicts an even closer link between convective rainfall and future pressure. Again, the best radius is used for the display but
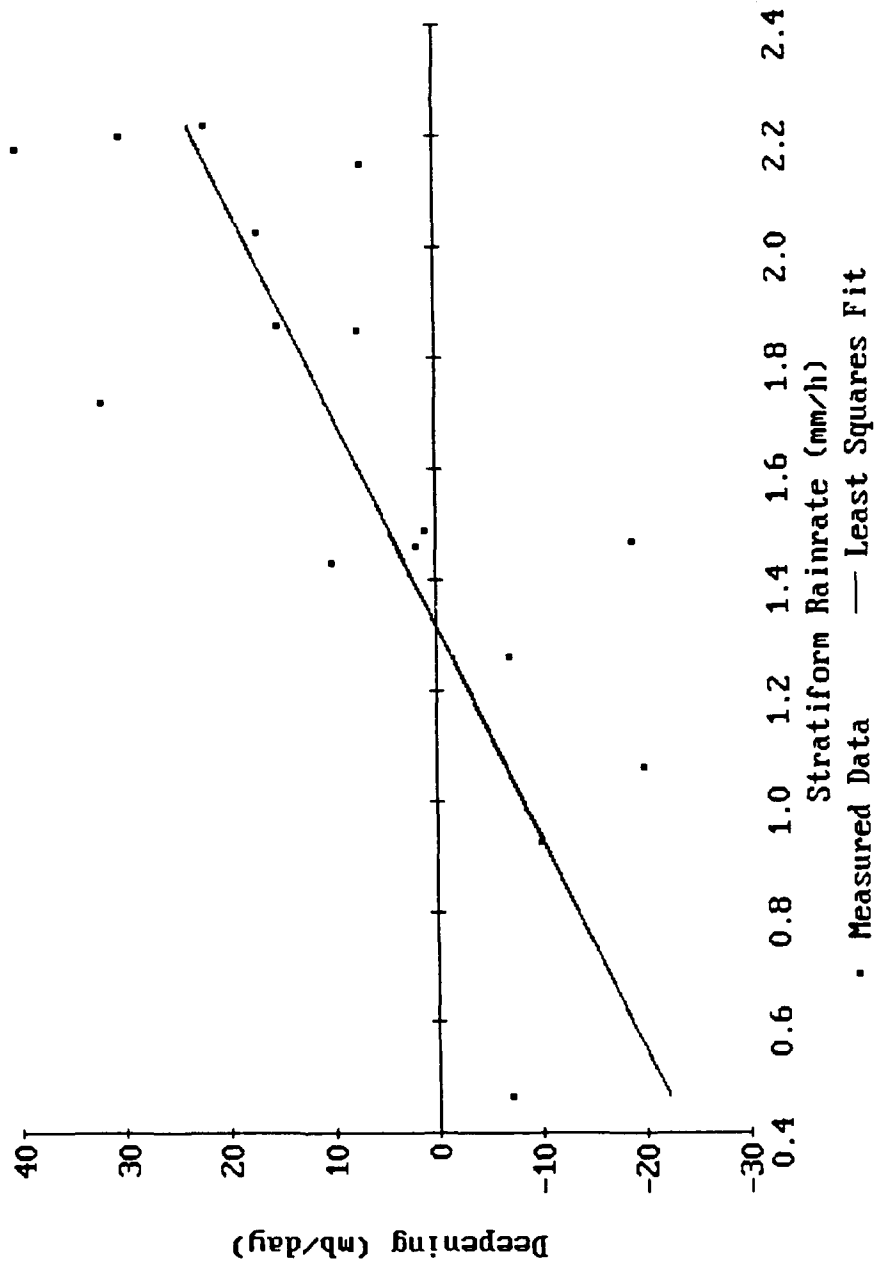
Figure 5.9. Scatter diagram of typhoon deepening as a function of mean stratiform rainfall within a 111 km box. Linear fit data: $D = 26.1R - 34.5$; R is in units [mm^3 h^{-1} x 10^{14}], D in [mb/day]. Heavy stratiform rainfall is tied to deepening.

Figure 5.10. Scatter diagram of typhoon 24-h central pressure as a function of mean stratiform rainfall within a 111 km box. Linear fit data: $P = -45.4R + 1033.5$; R is in units [$mm^3 h^{-1} \times 10^{14}$]. Note the fall of pressure as stratiform rainrates increased.

Figure 5.11. Scatter diagram of typhoon 24-h central
pressure as a function of mean convective rainfall rate
within a 28 km box. Note that the data gap from 0 to 3
mm/h is due to the definition of convective rainfall.
Linear fit data: P = -9.5R + 985.5; R is in units [mm^3
h^{-1} x 10^{14}]. The increased rainfall rates profoundly
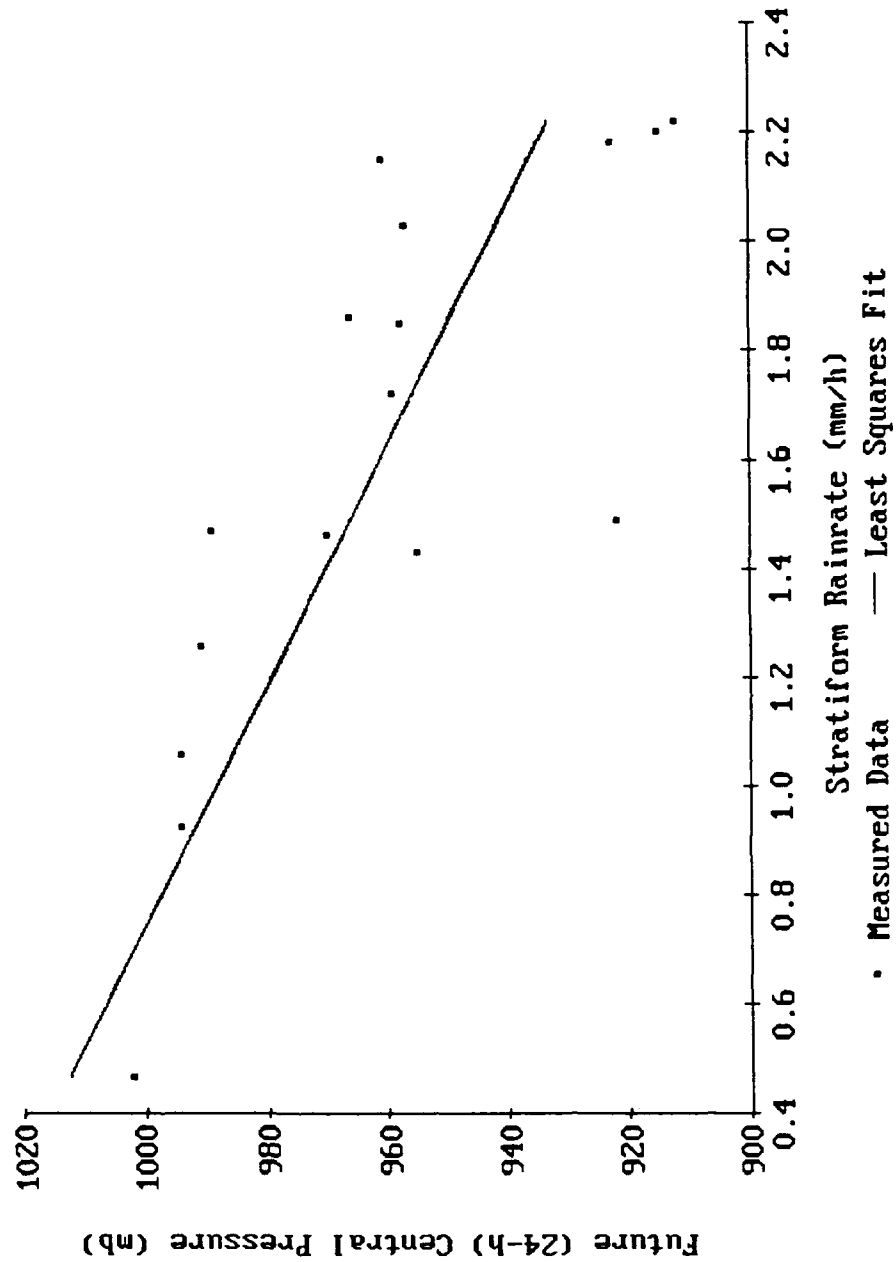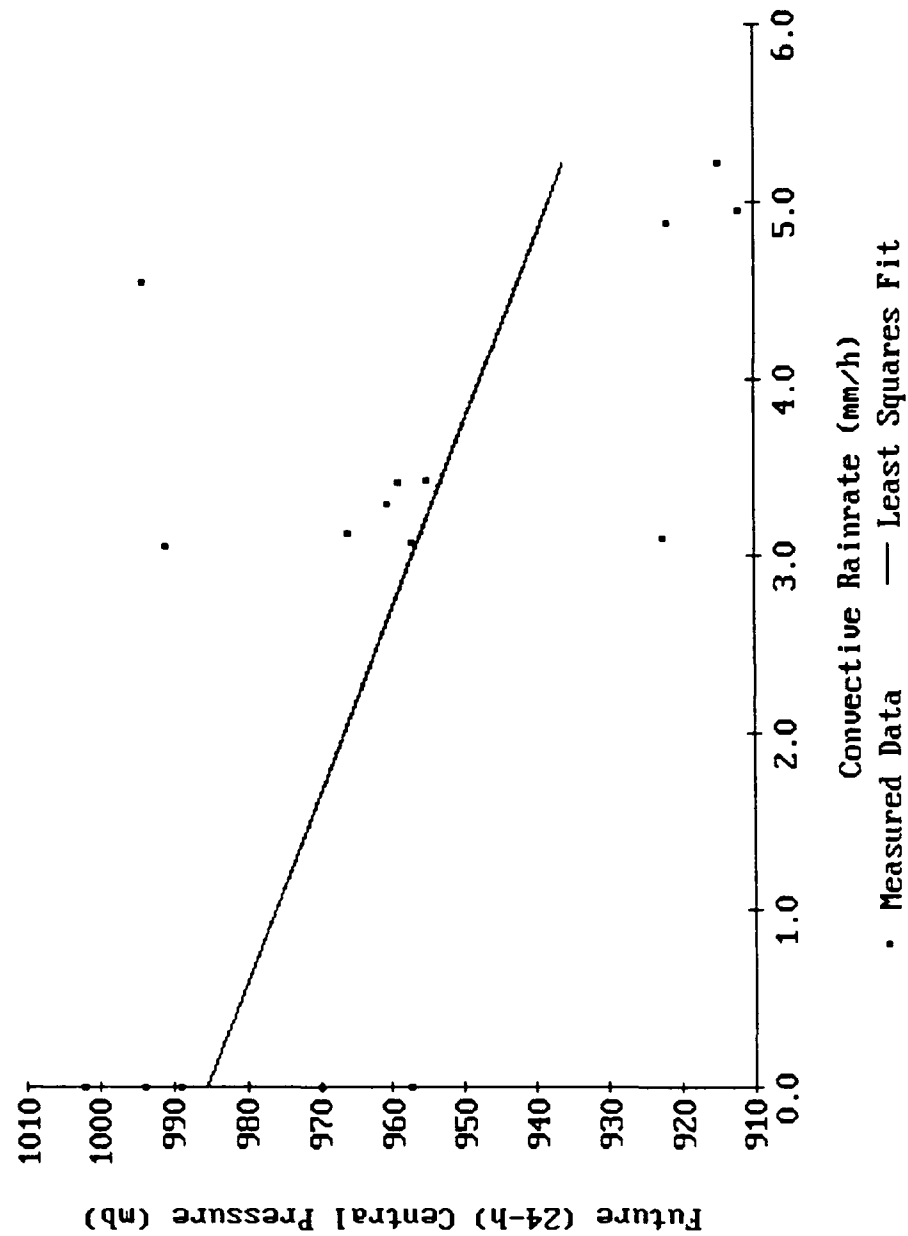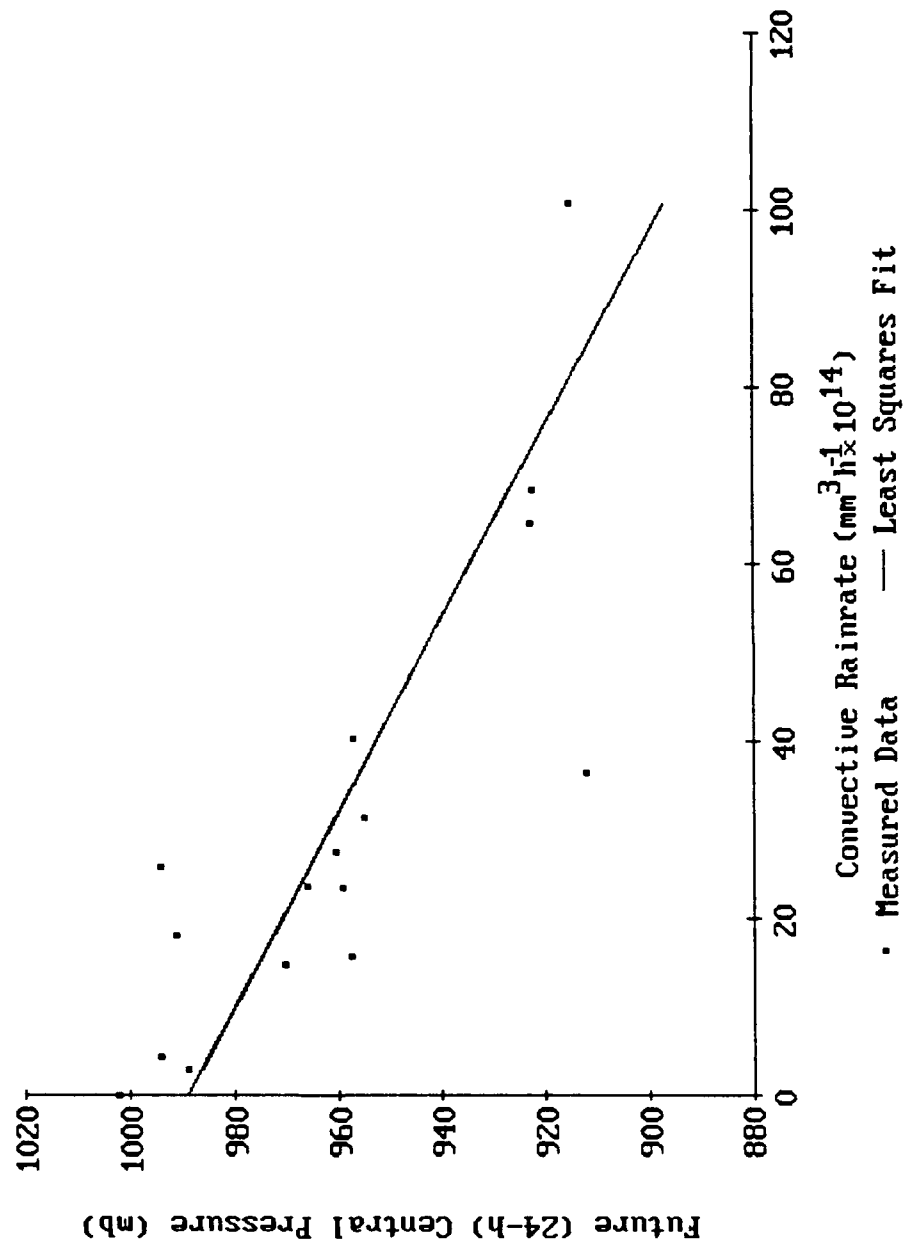influenced the 24-h pressure falls.

Figure 5.12. Scatter diagram of typhoon 24-h central pressure as a function of total convective rainfall rate within a 55.5 km box. Linear fit data: P = -.91R + 988.9; R is in units [mm³ h⁻¹ x 10¹⁴].

there were reasonably good fits for all radii out to and including 222 km (see Table 5.3). This again confirms the prominence (as seen in the cross-sectional views) of core convection in very low pressure storms.

Fig. 5.13 and 5.14 display 55.5 km total rainfall effects on typhoon development. As total (the sum of convective and stratiform) rainfall increased deepening increased and future pressure decreased. The correlation (r=-.88) is stronger for the future pressure but is good (r=.73) for deepening too. By adding stratiform rainfall to the convective of Fig. 5.12, a closer relationship to future pressure results.

Fig. 5.15 and 5.16 are both multiple plots. Fig. 5.15 is a scatter diagram of 55.5 km stratiform and 28 km convective mean rainrates vs. future central pressure. The combination of these two factors produces a three-way correlation coefficient of .73. This is less than the two-way correlation between stratiform rate and pressure (r=-.77). Indicating that, with regard to rainfall rates, stratiform rates in the core are more important than convective rates in the development of very low pressure storms.

The addition of convection to the stratiform rate of Fig. 5.15 is plotted in Fig. 5.16 where the solid line shows the fit (r=-.88) of mean total rainrate to future pressure. Thus the combination of rainrates gives the best results in the core. Fig. 5.16 combines

Table 5.3. The correlation of convective rainfall to 24-h central pressure for the radii listed. Radii represent whole boxes. Linear least squares fit data are also listed, where $Y = mX + b$. Units are: Y & b [mb], m [mb h mm^{-3} x 10^{-14}] , and X [mm^3 h^{-1} x 10^{14}].

Radius	r	m	b
28 km	-0.6	-1.74	973
55.5 km	-0.83	-0.91	989
111 km	-0.79	-0.327	998
222 km	-0.55	-0.095	989
333 km	-0.24	-	-
444 km	0.19	-	-

Figure 5.13. Scatter diagram of typhoon deepening as a function of total (convective and stratiform) rainfall within a 55.5 km box. Linear fit data: D = .54R − 21.4; R is in units [mm^3 h^{-1} x 10^{14}], D in [mb/day].
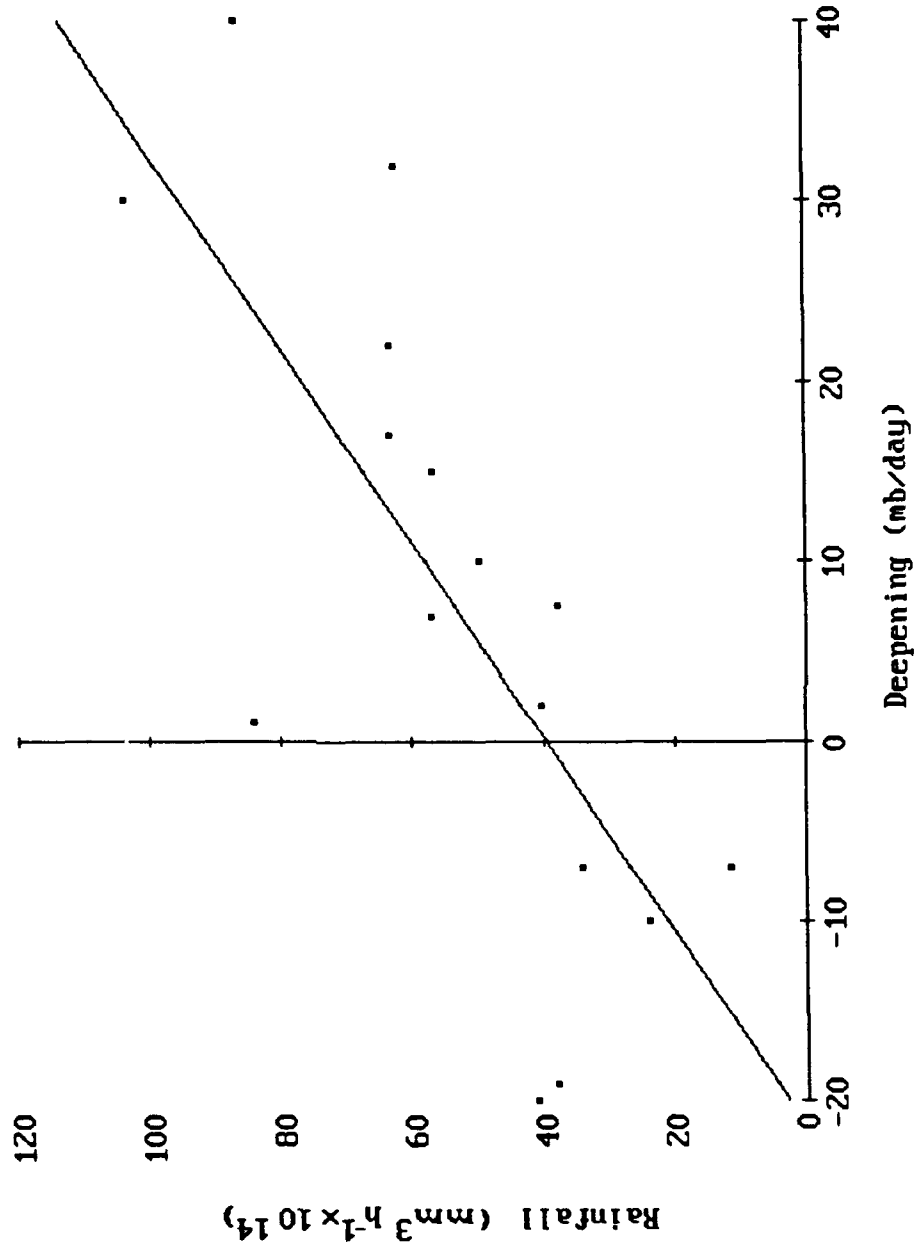
Rainfall vs. Future Pressure
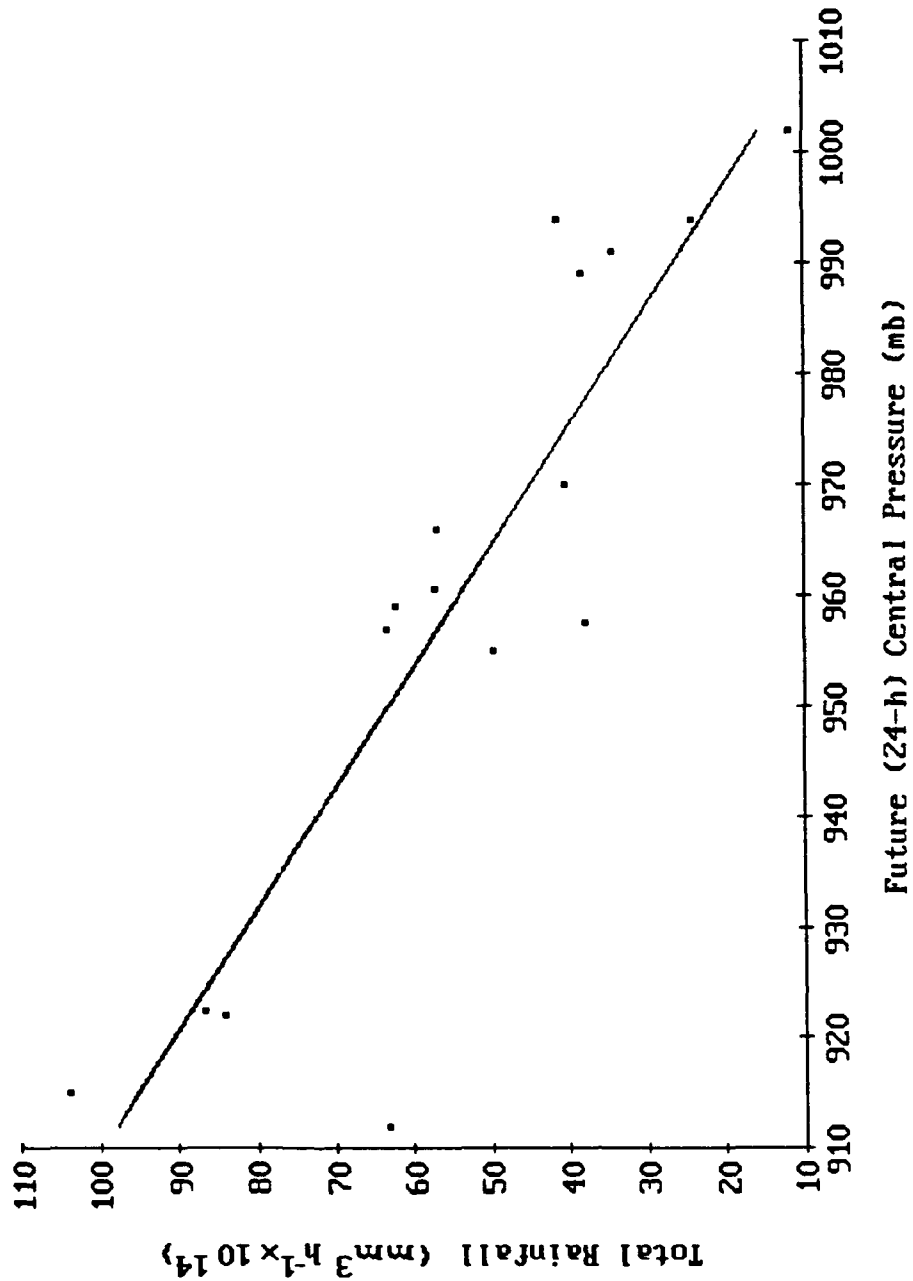
Figure 5.14. Scatter diagram of typhoon 24-h pressure as a function of total (convective and stratiform) rainfall within a 55.5 km box. Linear fit data: P = -1.09R + 988.9; R is in units [mm^3 h^{-1} x 10^{14}].

59

Figure 5.15. Dual scatter diagram of typhoon 24-h pressure as a function of mean stratiform rainrate within 55.5km boxes and mean convective rainrate within 28km boxes. Linear fit data: for 55.5 km boxes, P = -37.1R + 1026.5; for 28 km boxes, P = -9.5R + 985.5; R is in units [mm^3 h^{-1} x 10^{14}]. Note the association of increased rainrates and lower central 24-h pressures.
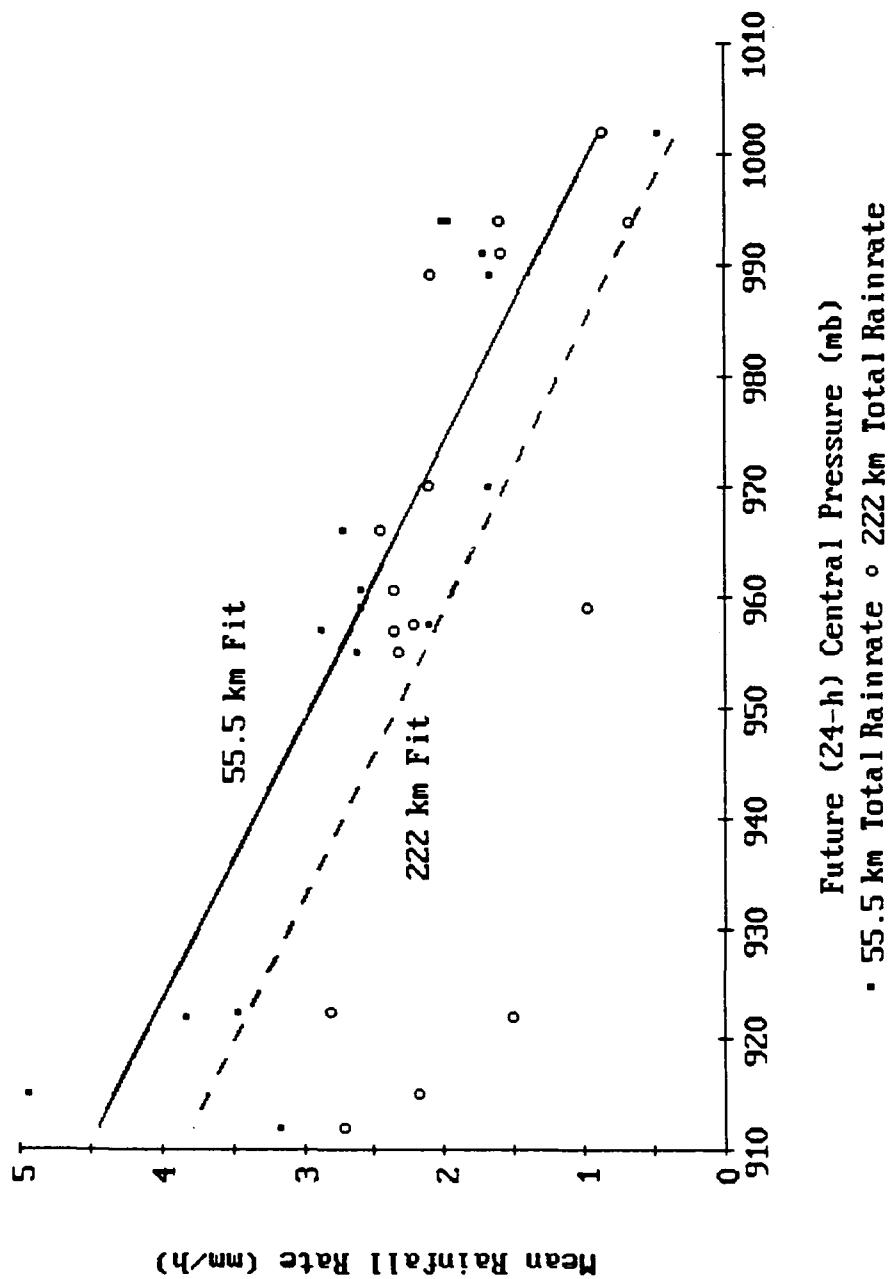
Figure 5.16. Dual scatter diagram of typhoon 24-h pressure as a function of total rainrates within 55.5 and 222 km boxes. Linear fit data: for 55.5 km boxes, $P = -1.09R + 1019$; for 222 km boxes, $P = -.070R + 1002$; R is in units [mm^3 h^{-1} x 10^{14}].

core precipitation rates with broader (222 km) rainfall rates. This combination produced a better fit (r=.9) than either of the components.

The reason stratiform rain (and rainfall rates) in the core is so important to future pressure is twofold. First, as stratiform rainrates approach 3 mm/h the rain becomes more like convective rain. This produces more release of latent heat than lower rates would, and thus contributes more to the total rainfall in the region (see Figs. 5.13 and 5.14).

Secondly, stratiform rain is a secondary indicator of convective activity, since much of the core non-convective rain precipitates from clouds with convective origins.

The aid that 222 km stratiform rainrates provides to 55.5 km total rainrates on future pressure can be in lowering the environmental pressure without establishing a barrier that convection would produce. Thus it releases latent heat without stopping the supply of latent heat (through high theta-e air) to the core. The result is a lower possible central pressure that was noted in the Northwest movers and, in general, in all the storms.

6. CONCLUSIONS

Microwave data from SSM/I have been used as both diagnostic and prognostic tools. The algorithm of Olson et al. (1990) was used to analyze the rainfall patterns of some of the 1987 - 88 western North Pacific Ocean typhoons. These rainfall rates and patterns were correlated to the typhoon's Dvorak intensities (both present and future) in search of prognostic aids.

Generally, SSM/I data proved useful in predicting the intensification trend and future central pressure of typhoons. It is hoped that forecasters can use the timely data from SSM/I (for rainrates) and OLS (for intensities) with the correlations obtained by this research to accurately predict typhoon behavior.

The number of peaks in the mean annular rainfall rates correlated strongly with the filling or deepening of a typhoon. This test categorized a storm as either strengthening or weakening. It could be used as a final discriminator if other tests are ambiguous.

The case studies produced some strong and revealing correlations, but the variance in the radii of maximum correlation makes forecast application of this test difficult. To best apply this test, more techniques must be developed to determine the effective radius of each storm.

Cross-sections of convective and stratiform rainfall revealed four distinct classes of storms. These classes are an improvement over the earlier stratification based on the mean annular rainfall peaks. Unfortunately, the patterns depicted in the cross-sections varied greatly from storm to storm, casting doubt on their applicability to prognostication. Further refinement is necessary to remove the subjectivity of pattern recognition.

The application of mean rainfall rates and PIP to storms moving in a northwesterly direction yielded reliable regression estimates. The twenty-four (24) hour central pressure of these storms can be calculated using our correlation values.

The research revealed some interesting characteristics of typhoons. These characteristics were previously observed by radar, by airborne sensors, and in numerical models of tropical cyclones. One of the characteristics is the effective radius of a cyclone. Although originally identified as the radius at which the internal actions of the storm are immune to the environment (Holland, 1983), it is used in this research as the radius demarcating regions in which released latent heat influences the typhoon differently. For example, in typhoon Dinah rainfall within 111 km of the eye tended to reduce the central

pressure, but rainfall outside 222 km increased central pressure.

This research emphasized the importance of the stratiform rainfall in typhoon development, and its proportionately high contribution to the total rainfall. Furthermore, too much convection in the outer region of a storm seems to have a detrimental effect on typhoon development.

A third finding was the significance of a strong convective core. High PIP in the inner region was correlated to developing storms, though probably not as important as overall distribution of rainfall (as signified by moderate correlation coefficients).

A fourth phenomenon was the demonstration of the barrier effect by the examination of mean annular rainfall rates (MARR) and PIP. If a second convective band was indicated by a strong PIP in the outer region, or by the existence of multiple MARR peaks, the storm weakened. This is akin to the action of a barrier preventing the energy rich environmental air from reaching the core.

While this research clarified the character of typhoon precipitation and yielded some forecast techniques, much remains to be explored with SSM/I. Work begs to be done with the data presented in this thesis; other stratifications should be applied such as sea surface temperatures, Empirical Potential

Intensity (Jorgensen, 1984), rainfall rate asymmetries (inner vs. outer or right vs. left), and adjustments to the box orientation (e.g., front and back instead of right and left).

Improvements could be made to the application of the rainfall rate algorithm. This could be done by including a land/sea screen which would apply the proper regression to the SSM/I data. Some of the ambiguities encountered in this research could possibly be resolved by eliminating the land contamination.

As always, this research could be furthered by an improved data base. With an increased data set such things as northeast moving, South Pacific Ocean, and Atlantic Ocean storms could be examined.

With enough map times, some climatological inferences could be made. With these inferences, a model of latent heat release due to tropical storms could be included in a global climate model. The coverage of satellite borne microwave sensors and their correlation to environmental parameters would make SSM/I a reasonable choice for inclusion into the model.

Indeed, the coverage, timeliness, reliability, and economy of satellite borne microwave sensors makes them an item of interest to researcher and forecaster alike.

REFERENCES

Adler, R.F., R.A. Mack, N. Prasad, H.-Y.M. Yeh, and
    I.M. Hakkarinen, 1990: Aircraft microwave
    observations and simulations of deep convection
    from 18 to 183 GHz. Part I: Observations.
    Journal of Atmospheric and Oceanic Technology, 7,
    377-391.

Burpee, R.W., and M.L. Black, 1989: Temporal and
    spatial variations of rainfall near the centers of
    two tropical cyclones. *Mon. Wea. Rev.*, 117, 2204-
    2218.

Carr, L.E. III, and R.L. Elsberry, 1990: Observational
    evidence for predictions of tropical cyclone
    propagation relative to environmental steering.
    J. Atmos. Sci., 47, 542-546.

Dvorak, V.F., 1984: Tropical cyclone intensity
    analysis using satellite data. NOAA technical
    report NESDIS 11. US Department of Commerce,
    Washington D.C., 47pp.

Fiorino, M., and R.L. Elsberry, 1989a: Contributions
    to tropical cyclone motion by small, medium and
    large scales in the initial vortex. *Mon. Wea.
    Rev.*, 117, 721-727.

_____, and _____, 1989b: Some aspects of
    vortex structure related to tropical cyclone
    motion. *J. Atmos. Sci.*, 46, 975-990.

Glass, M., and G.W. Felde, 1989: Structure of tropical
    cyclones and surrounding regions as determined
    from OLS and SSM/I imagery analysis. *Preprints.
    Fourth Conference on Satellite Meteorology and
    Oceanography*, San Diego, California, American
    Meteorology Society, Boston, Ma., 35-38.

Hoffman, C.W., V.G. Patterson, and D.J. McMorrow, 1988:
    1987 annual tropical cyclone report. Joint
    Typhoon Warning Center, Guam, Mariana Islands,
    213pp.

Holland, G.J., 1983: Tropical cyclone motion:
    Environmental interaction plus betta effect. *J.
    Atmos. Sci.*, 40, 328-342.

Hollinger, J.T., K. Lo, G. Poe, R. Savage, and J.
    Peirce, 1987: Special sensor microwave/imager
    user's guide. Dept of the Navy, Naval Research
    Lab., Washington, D.C., 120 pp.

Jorgensen, D.P., 1984: Mesoscale and convective scale characteristics of mature hurricanes. Part I: General observations by research aircraft. *J. Atmos. Sci.*, **41**, 1268-1285.

Merril, R.T., 1988: Environmental influences on hurricane intensification. *J. Atmos. Sci.*, **45**, 1678-1687.

Olson, W.S., F.J. Fontaine, W.L. Smith, and T.H. Achtor, 1990: Recommended algorithms for the retrieval of rainfall rates in the tropics using SSM/I (DMSP-8). Manuscript, Univ. of Wisconsin, Madison. 10pp.

Plante, R.J. and D.J. McMorrow, 1989: 1988 annual tropical cyclone report. Joint Typhoon Warning Center, Guam, Mariana Islands, 216pp.

Powell, M.D., 1990: Boundary layer structure and dynamics in outer hurricane rainbands part I: Mesoscale rainfall and kinematic structure. *Mon. Wea. Rev.*, **118**, 891-917.

_____, and P.G. Black, 1984: Airborne Doppler radar observations of the boundary layer of Hurricane Debby (1982). *Preprints, 22nd Conf. on Radar Meteorology*. Zurich, Switzerland, Amer. Meteor. Soc., Boston, 584 - 588.

Rao, A.V.R.K., R.R. Kelkar, and P.A. Arkin, 1989: Estimation of precipitation and outgoing longwave radiation from INSAT-IB radiance data. *Mausam*, **40**, 123-130.

Rao, G.V., 1970: An analytical study of the differential frictional effect on vortex movement. *Mon. Wea. Rev.*, **98**, 1332-135.

_____, E.J. Ciardi and D.K. Rhudy, 1989: Comparison of SSM/I rainrates and surface winds with the corresponding conventional data in the north west pacific typhoons. *Preprints. Fourth Conference on Satellite Meteorology and Oceanography*, San Diego, California, American Meteorology Society, Boston, Ma., 104-107.

Rhudy, D.K., 1989: Applications of microwave radiometric measurements to infer tropical cyclone intensity and strength. M.S. Thesis, St. Louis University, St. Louis, Mo., 95 pp. Available from University Microfilms, Ann Arbor, Mi.

Spencer, R.W., H.M. Goodman, and R.E. Hood, 1989:
     Precipitation retreval over land and ocean with
     SSM/I: Identification and characteristices of the
     scattering signal. *Journal of Atmospheric and
     Oceanic Technology*, 6, 254-273.

Staff, 1988: Tropical cyclones in 1987. Royal
     Observatory, Hong Kong, 73pp.

Steranka, J., E.B. Rodgers, and R.C. Gentry, 1986: The
     relationship between Satellite measured convective
     bursts and tropical cyclone intensification. *Mon.
     Wea. Rev.*, 114, 1539-1546.

Willoughby, H.E., 1988: Dynamics of the tropical
     cyclone core. *Aust. Met. Mag.*, 36, 183-191.

BIOGRAPHY OF THE AUTHOR

Paul Douglas MacArthur was born on 16 June 1956 in Ft. Lawton, Washington. He graduated from Moscow High School in Moscow, Idaho in 1974. After spending a tour in the Army, he attended Washington State University majoring in Mechanical Engineering. Upon graduation in February, 1984, he joined the United States Air Force and was commissioned on 4 May, 1984. He spent the next 12 months attending San Jose State University, San Jose, California in basic meteorology studies. From San Jose he moved to Plattsburg, New York where he worked for over a year as Wing Weather Officer. His next assignment was for three years in Ramstein, Germany, where he served as weather officer until being assigned to attend graduate school in Saint Louis University in August, 1989. The author is married to the former Tammy Lynn Manley.